JOURNAL OF MATERIALS SCIENCE 29 (1994) 3128–3150

Fabrication of particulate aluminium–matrix composites by liquid metal infiltration

SHY-WEN LAI, D. D. L. CHUNG
Composite Materials Research Laboratory, State University of New York at Buffalo, Buffalo, New York 14260-4400, USA

Aluminium–matrix composites were fabricated by liquid metal infiltration of porous particulate reinforcement preforms, using AlN, SiC and Al_2O_3 as the particles. The quality of the composites depended on the preform fabrication technology. In this work, this technology was developed for high-volume fraction (up to 75%) particulate preforms, which are more sensitive to the preform fabrication process than lower volume fraction whisker/fibre preforms as their porosity and pore size are much lower. The technology developed used an acid phosphate binder (with P/Al molar ratio = 23) in the amount of 0.1 wt% of the preform, in contrast to the much larger binder amount used for whisker preforms. The preforms were made by filtration of a slurry consisting of the reinforcement particles, the binder and carrier (preferably acetone), and subsequent baking (preferably at 200 °C) for the purpose of drying. Baking in air at 500 °C instead of 200 °C caused the AlN preforms to oxidize, thereby decreasing the thermal conductivity of the resulting Al/AlN composites. The reinforcement-binder reactivity was larger for AlN than SiC, but this reactivity did not affect the composite properties due to the small binder amount used. The Al/AlN composites were superior to the Al/SiC composites in the thermal conductivity and tensile ductility. The Al/Al_2O_3 composites were the poorest due to Al_2O_3 particle clustering.

1. Introduction

The infiltration of a liquid metal infiltration into a porous reinforcement preform is one of the most economical methods for producing metal–matrix composites (MMCs). The quality of an MMC depends on that of the preform, in addition to that of the reinforcement. The preparation of a preform involves the use of a slurry consisting of a binder, a liquid carrier and reinforcement, and subjecting the slurry to filtration, as in paper making. Subsequently the preform is dried and heat-treated; the heat treatment is to allow the binder to become the desired phase and possibly to react with the reinforcement to the desired degree, so as to enhance the binding ability of the binder. The choice of binder, the binder amount and the preform heat treatment conditions are critical to the quality of the preform. A preform of good quality refers to one which is mechanically strong (so that the preform does not change dimensions during the subsequent liquid metal infiltration) and is easy for the liquid metal to infiltrate completely. The mechanical strength of the preform increases with the binder amount in the preform, whereas the ease of liquid metal infiltration decreases with increasing binder amount. Thus an optimum binder amount is preferred. This optimum depends on the shape and volume fraction of the reinforcement. A low volume fraction means the existence of larger open channels for liquid metal infiltration, so a larger binder amount may be tolerated without decreasing the ease of infiltration. Because of the nature of the paper-making process used for making preforms, preforms with whiskers or fibres as the reinforcement tend to have a lower volume fraction than those with particles as the reinforcement. As a result, the binder technology is less critical in the case of whisker or fibre preforms than in the case of particulate preforms.

Silica colloid is the most commonly used binder for preform fabrication. The acid phosphate binder (made from aluminium hydroxide and excess phosphoric acid) is a recent development that has been shown to be superior to the silica colloid, as demonstrated for the case of silicon carbide whiskers (SiC_w) as the reinforcement [1–4]. The superiority is in terms of the mechanical properties of the preform and the high temperature resistance of the resulting aluminium–matrix composite. In this work, the acid phosphate binder was applied to particles (rather than whiskers) as the reinforcement and to reinforcements other than SiC. As the binder-reinforcement reactivity affects the binding ability, the investigation of reinforcements of various reactivities is relevant to the broad applicability of the acid phosphate binder. This work has resulted in the development of a preform preparation process for particulate preforms with the acid phosphate binder. Moreover, the binder phases and binder-reinforcement reaction products have been identified for each of three kinds of particles, i.e. SiC, AlN and Al_2O_3.

MMCs of high thermal conductivity and low

0022–2461

thermal expansion are needed for heat sinks, back planes, housings and substrates for high-density electronics. MMCs for these applications are most commonly made by the infiltration of a liquid metal into a porous reinforcement preform, as shaping can be conveniently achieved by machining the preform prior to liquid metal infiltration. The preform baking conditions may affect the thermal conductivity of both preforms and composites, as the cleanliness of the reinforcement surface or the reinforcement–matrix interface may be critical to the thermal conductivity. The preform baking conditions (temperature and environment) are particularly critical if the reinforcement, such as AlN, is sensitive to moisture, oxidation or acid. One objective of this work is to investigate the effects of the preform baking conditions on the thermal conductivity of Al/AlN and Al/SiC composites and to improve the thermal conductivity of Al/AlN composites by using the optimum preform baking conditions.

The preform baking conditions also affect the mechanical properties of the MMCs. It has been observed in [1–4] that SiC_w preforms baked in air at 500 °C resulted in Al/SiC_w of the maximum tensile strength. In this work, the preform baking conditions of 200 °C in air, 510 °C in air, and 500 °C in vacuum were used to investigate the effect of preform baking on the mechanical properties of the resulting Al/AlN composites.

2. Experimental procedure and results

2.1. Particulate reinforcements

Three kinds of particulate reinforcements were used, namely AlN, SiC and calcined Al_2O_3. The AlN (AlNel grade A-100) and SiC (#1200-W) particles were kindly provided by Advance Refractory Technologies, Inc. (ART) and Electro Abrasives, Inc., respectively. The calcined alumina particles. (A-17) were obtained from Aluminium Company of America (ALCOA). The AlN particle sizes ranged from 2 to 7 μm, with a mean at 3.7 μm, but coarse particles of up to 12 μm were also present. The SiC particle size ranged from 1 to 10 μm, with a mean of 3 μm. The alumina particle size had an average of 3.0 to 3.5 μm. The properties of the three kind of powders are listed in Table I. The composition of AlN was 66.0% Al, 33.0% N, 0.07% C, 1.0% O, 0.005% Fe and 0.005% Si. The composition of SiC was 98.5% SiC, 0.5% SiO_2, 0.3% Si, 0.08% Fe, 0.1% Al, 0.3% C. The calcined alumina contained 99.7% Al_2O_3, 0.08% Na_2O, 0.02% SiO_2, 0.01% Fe_2O_3 and 0.001% B_2O_3.

Fig. 1 shows SEM micrographs of AlN, SiC and calcined Al_2O_3 powders (without any binder, prior to preform fabrication). Both AlN and SiC had 'clean' particle surfaces. However, the calcined Al_2O_3 exhibited very fine particles surrounding each Al_2O_3 particle, so that particle clustering occurred and resulted in little space for liquid metal infiltration. Fig. 2 shows the Al_2O_3 particle clustering, which resulted in weak Al_2O_3 composites. No such particle clustering was found for the AlN and SiC particles.

2.2. Binders

Two kinds of binders, namely a silica colloid binder and an acid phosphate binder, were used for preform preparation. The silica colloid (30 wt % silica in water) was obtained from EM Science Co. Precipitation of silica was observed when the silica colloid was mixed with acetone (a carrier that is compatible with AlN, which reacts with water) at a silica colloid/acetone volume ratio of 1/45 or 1/10. This precipitation made the silica binder not attractive, as it resulted in preforms that were much weaker than those obtained with the phosphate binder. That the use of the phosphate binder, rather than the silica colloid binder, resulted in superior mechanical properties of the preforms and of the composites has been demonstrated in [1–4] and confirmed in this work. Unless mentioned otherwise, the phosphate binder was used for the preform preparation.

The phosphate solutions were prepared by mixing one part of aluminium hydroxide ($Al(OH)_3$, obtained from J. T. Baker Chemical Co.) with phosphoric acid (H_3PO_4, 85% Technical Grade, Riverside Chemical Co.), so that the solutions had the P/Al molar ratio of 23. Following [1–4], the phosphate binder of the P/Al molar ratio of 23 is denonated as A23. After mixing the aluminium hydroxide with phosphoric acid, the slurry was stirred and heated to 150 °C. It was held at ~ 150 °C until all the aluminium hydroxide ($Al(OH)_3$) was dissolved.

In order to understand the binder science, the phosphate A23 binder was heat-treated in the absence of the reinforcement, but in the same manner as in the

TABLE I Properties of AlN, SiC and Al_2O_3 powders

	AlN	SiC	Al_2O_3
Mean particle size (μm)	3.7	3.0	3.0–3.5
Oxygen content (%)	1.0	–	–
Specific surface area ($m^2\ g^{-1}$)	2.5–4.0		3
Density ($g\ cm^{-3}$)	3.26	3.18	3.97
Young's modulus (GPa)	345	400–440	379
Electrical resistivity (Ω cm)	$\geqslant 10^{13}$	–	$\geqslant 10^{14}$
Dielectric constant	8.2–9.0	–	9.3
Thermal conductivity ($W\ m^{-1}\ K$)	160–220	90	20
Coefficient of thermal expansion (μm m^{-1} C)	3.3	3.4	7.0
Crystal structure	Hexagonal	Hexagonal	Corundum

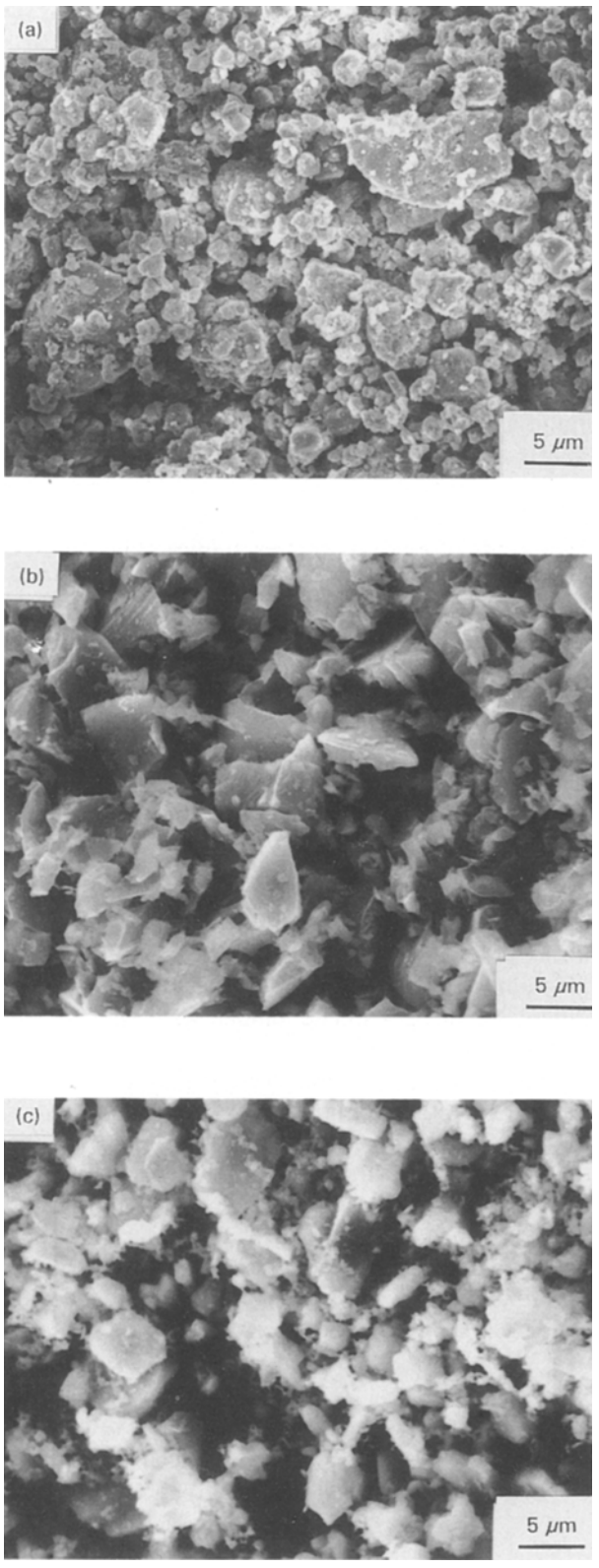

Figure 1 SEM micrographs of AlN, SiC and Al_2O_3 powders (without any binder). (a) AlN, (b) SiC, (c) Al_2O_3.

presence of the reinforcement during preform preparation. Subsequent to the heat treatment, the binder was characterized.

Drying of the A23 phosphate binder was accomplished by heating the binder first at 200 °C for at least 1 week and then at either 510 or 800 °C for 3 h. After heating at 200 °C, the phosphate binder was still not dried and resembled a viscous emulsion. This was due

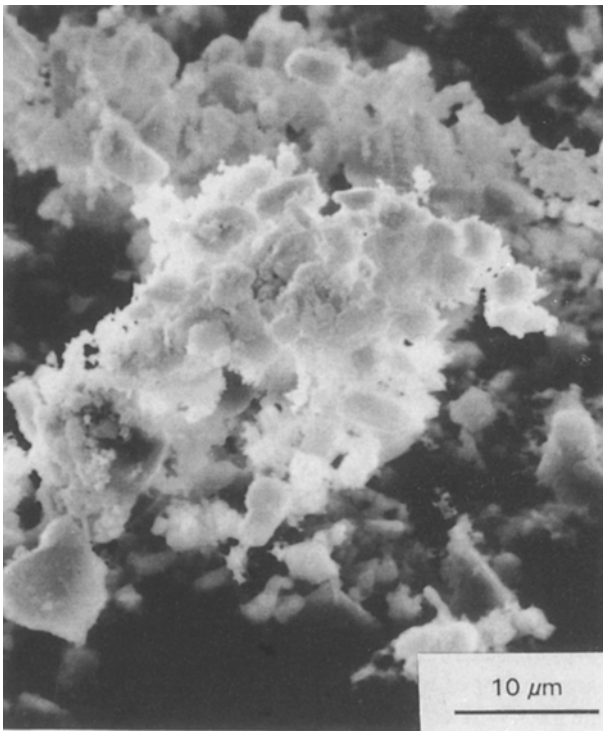

Figure 2 SEM micrographs of an Al_2O_3 particle cluster (without any binder).

to the fact that a large amount of phosphate binder was placed in the glass container with a small interface area between the phosphate binder and air. If a small amount of phosphate binder had been placed in a large glass container, the binder would have been dried after baking at 200 °C. The incompletely dried binder was amorphous while the dried one was crystalline. The latter is more suitable for the preparation of preforms as a large amount of interface area exists between the binder and the reinforcement in a preform.

The temperature was increased from 200 °C to either 510 or 800 °C at a heating rate of 1.4 °C min^{-1}, kept at 510 or 800 °C for 3 h, and then furnace-cooled to room temperature.

Fig. 3 shows X-ray diffraction (XRD) patterns of the phosphate binder, which by itself had been baked at

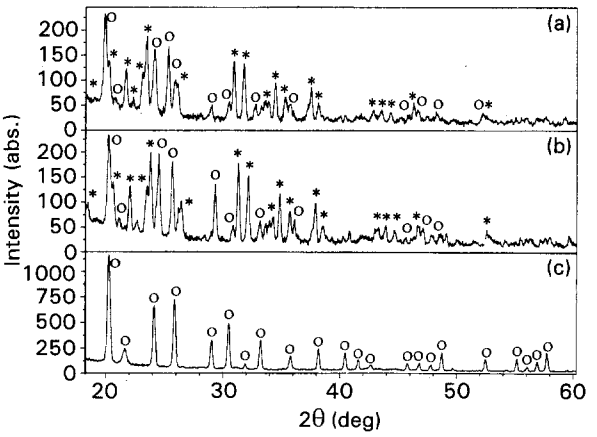

Figure 3 XRD patterns of the phosphate binder itself baked at (a) 200, (b) 510 and (c) 800 °C for 24 h. ○, $Al(PO_3)_3$ (A); *, $Al(PO_3)_3$ (B).

200, 510 and 800 °C for 24 h. The binder baked at 200 °C showed similar diffraction patterns to that baked at 510 °C, indicating that the crystallization occurred even at 200 °C. This is in contrast to results in [1–4], which showed that the same binder was amorphous after heating at 200 °C. This may be ascribed to the fact that in the previous work the binder was not completely dried, whereas the binder was completely dried in the present research. After drying of the phosphate binder at either 200 or 510 °C, both type A and type B aluminium metaphosphate ($Al(PO_3)_3$) phases formed. The amounts of type A and type B aluminium metaphosphate ($Al(PO_3)_3$) phases were similar for both baking temperatures of 200 and 510 °C. When baked at 800 °C, the binder formed predominantly type A aluminium metaphosphate ($Al(PO_3)_3$).

2.3. Preform preparation

The AlN, SiC and Al_2O_3 preforms were prepared by wet forming, which involved compressing in a die a slurry containing AlN, SiC or Al_2O_3 powder, a liquid carrier (acetone) and the phosphate binder. Acetone was used because it is non-aqueous and AlN reacts with H_2O to form $Al(OH)_3$ and NH_3. The die allowed excessive liquid to be squeezed out from the slurry and formed a wet cake. As shown in Table II, AlN or SiC preforms were prepared using the A23 acid phosphate or silica colloid as the binder and using water or acetone as the carrier. Both binders were completely miscible with water. The acid phosphate was miscible with acetone without precipitation (at, for example, a binder/acetone ratio of 1/45). However, silica colloid encountered severe precipitation upon mixing (at a binder/carrier ratio of 1/10 or 1/45) with acetone. The precipitates formed a network, which was believed to be silica. A silica colloid binder/carrier ratio of 1/10 was used only for preform preparation (not for MMC fabrication due to non-infiltration).

The use of the phosphate as a binder and acetone as the carrier resulted in the highest compressive strength for both AlN and SiC preforms (Table II). For SiC preforms, the use of water (instead of acetone) and the phosphate binder resulted in a slightly lower compressive strength. The use of silica colloid (instead of the phosphate) and water (instead of acetone) resulted in SiC preforms without cracking. However, microstructural observations of the resulting Al/SiC composite revealed porosity due to incomplete infiltration. The use of silica colloid (instead of the phosphate) in acetone resulted in the lowest compressive strength due to severe precipitation. For AlN preforms, the use of water (instead of acetone) together with silica colloid (instead of the phosphate) resulted in a much lower compressive strength than the use of acetone together with the phosphate binder; this was due to the AlN reaction with water. The AlN preforms prepared with either phosphate + water or silica colloid + acetone were prone to cracking during preform heating as well as during liquid metal infiltration. For silica colloid and acetone, the origin of preform cracking was due to severe silica precipitation and the resulting depletion of the silica binder. For the case of

TABLE II Observations and compressive strength of AlN and SiC preforms using various binders and carriers[a]

Binder	Carrier	Filler	Observations	Compressive strength (MPa)
A23 acid phosphate (1)	Acetone (45)	AlN	No binder precipitation in carrier Low viscous slurry Preform suitable for MMC fabrication	5.12 (0.76)
A23 acid phosphate (1)	Acetone (45)	SiC	No binder precipitation in carrier Very viscous slurry Preform suitable for MMC fabrication	3.83 (0.36)
A23 acid phosphate (1)	Water (45)	AlN	No binder precipitation in carrier Viscous slurry, NH_3 gas bubbles in slurry Preform cracks during baking No infiltration in MMC fabrication	2.72 (0.01)
A23 acid phosphate (1)	Water (45)	SiC	No binder precipitation in carrier Very viscous slurry	3.23 (0.16)
Silica colloid (1)	Acetone (10)	AlN	Severe binder precipitation in carrier Viscous slurry Surface cracks during baking Incomplete infiltration in MMC fabrication	2.91 (0.42)
Silica colloid (1)	Acetone (10)	SiC	Severe binder precipitation in carrier Very viscous slurry Surface cracks during baking	3.02 (0.33)
Silica colloid (1)	Water (12)	SiC	No binder precipitation in carrier Very viscous slurry Incomplete infiltration in MMC fabrication	

[a] Preforms were baked at 510 °C in air. Volume fractions were 55% for either AlN or SiC preforms. Indicated in parentheses in the first two columns are the mixing ratios in volume. Indicated in parentheses in the last column is the standard deviation of the compressive strength.

phosphate and water, the origin of AlN preform cracking was due to the NH_3 gas evolution. Such AlN preforms would have exhibited higher compressive strengths if the cracking were diminished. Microstructural observations of the resulting Al/AlN composites revealed cracks and porosity due to incomplete infiltration. This caused the resulting Al/AlN composite to have inferior mechanical properties. Therefore, only the combination of the phosphate binder and acetone was subsequently used for the preparation of MMCs. Two carrier/binder ratios of 45:1 and 10:1 (by volume) were used in the study of preform preparation. Only the preforms made with a carrier/binder ratio of 45:1 were used for fabricating composites, as this amount of binder was sufficient to maintain rigidity in the preform and an excessive amount of binder (as in the case of a carrier/binder ratio of 10:1) caused the preform to be not porous enough for subsequent liquid metal infiltration even at 41 MPa.

The volume fraction of reinforcement in the preforms can be controlled by adjusting the compressive pressure during wet forming, the reinforcement aspect ratio, the reinforcement particle size and size distribution and the rheology of the carrier/binder solution. However, only the pressure was used to vary the reinforcement volume fraction in this work; the range of volume fraction achieved was quite narrow, as shown in Table III for the AlN preforms. The minimum volume fraction achieved with this method was 55 vol % for both AlN and SiC preforms and was 60 vol % for Al_2O_3 preforms.

The preforms used for the composite fabrication were cylinders, 4.0 cm in diameter, with a height-to-diameter ratio of 0.3–0.5. However, the preforms used for the investigation of the reinforcement/binder reaction and compressive strength were cylinders 1.25 cm in diameter, with a height-to-diameter ratio of 1. In this paper, 'composite cylinder' refers to the metal-infiltrated preform.

Although all the experimental work described in this paper involved preforms prepared by the wet-forming technique, the dry-powder compact method had been tried and resulted in preforms that were fragile and non-uniform in the reinforcement distribution.

After removal from the die, the AlN, SiC or Al_2O_3 compact was dried in a fume hood at room temperature for 3 h. After drying, which removed most of the acetone, the preform was fired by (i) placing the preform in a furnace at room temperature; (ii) heating to 510 °C at a controlled rate of 1.4 °C min^{-1}; (iii) holding at 510 °C for 3 h; and (iv) cooling in the closed furnace. Excessive heating and cooling rates and a non-uniform temperature distribution in the furnace had to be avoided, as they would cause quick evolution of acetone and thermal stresses, thus resulting in cracking during the firing. Fig. 4a shows a tomography scan photograph of an AlN preform in which thermal cracking existed in the bottom portion of preform. A 45° crack from the bottom edge indicated that the preform failed in shear. No such cracking was found in the well-formed preforms (Fig. 4b).

TABLE III Effect of applied pressure (during wet forming) on the AlN volume fraction of the resulting preform

Applied pressure (MPa)	Vol % AlN
0	55
7.8	58–59
2 × 7.8	60.5
3 × 7.8	61.5
4 × 7.8	62.3
5 × 7.8	65.3

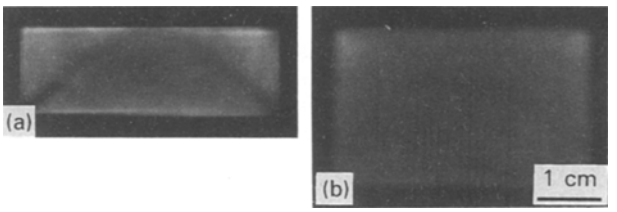

Figure 4 (a) Tomography scan photograph of an AlN preform showing 45° thermal cracking starting from the bottom edge portion of the preform. (b) Tomography scan photograph of a well-baked preform.

Instead of heating at 510 °C, some preforms were heated at 200 °C for 24 h or at 800 °C for 3 h, in order to study the effect of temperature on the morphology of the binder and the preforms. Unless noted otherwise, all preform heating was conducted in air. SEM was also used to observe the distribution of the binder in the preform.

In order to study the reaction between the reinforcement (AlN, SiC or Al_2O_3) and the phosphate binder, each kind of reinforcement was mixed with the phosphate binder without the acetone carrier and similarly baked using the above-mentioned baking procedure. The mixture was then ground into powders for XRD investigation.

2.4. Preform morphology and binder distribution

Although preforms fabricated with the carrier/binder ratio of 45:1 showed no distinct binder under the SEM, the preforms fabricated with the carrier/binder ratio of 10:1 showed the binder distinctly under the SEM. Fig. 5a, at the centre and lower left regions, shows more binder in the edge of the AlN preform fabricated with the carrier/binder ratio of 10:1 and baked at 200 °C than in the centre of the same preform (Fig. 6b). The phosphate binder in the preform appeared spherical and smooth in morphology. At the centre, the preform showed no distinct binder, just as for preforms with a carrier/binder ratio of 45:1.

Fig. 6 shows SEM photographs of AlN preforms fabricated with a carrier/binder ratio of 10:1 after baking in air at 200 and 510 °C, respectively. Only the edges of both preforms were examined as less binder was present in the centre regions. Some binder existed

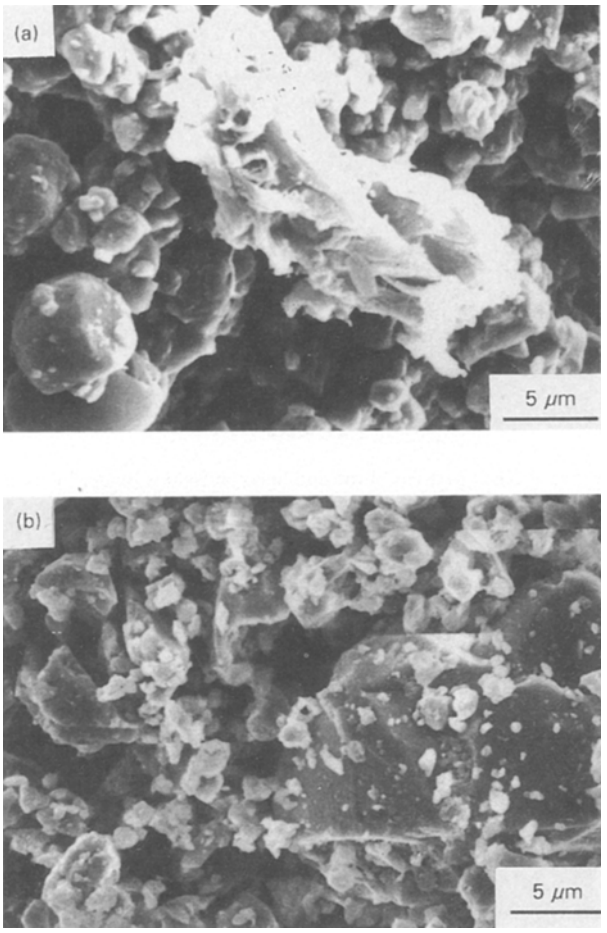

Figure 5 SEM micrographs of an AlN preform fabricated with a carrier/binder ratio of 10:1 and baked at 200 °C. (a) Edge of the preform showing spherical binder precipitates of size ~ 5 μm. (b) Centre of preform showing no distinct binder.

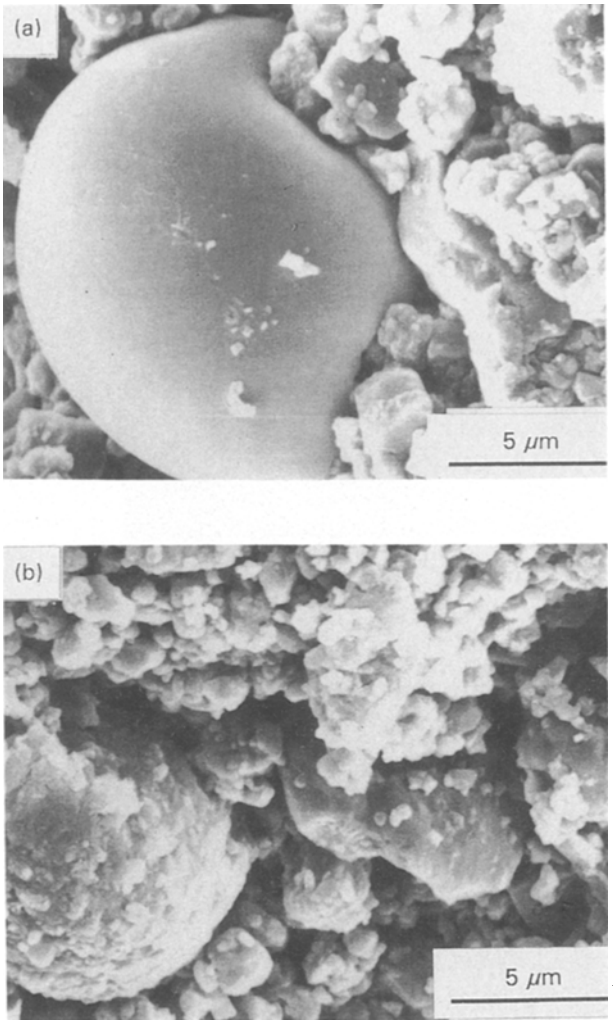

Figure 6 SEM micrograph of AlN preforms (at the edge) fabricated with a carrier/binder ratio of 10:1 and baked at (a) 200 °C, (b) 510 °C.

separately in spherical shapes and enclosed fine AlN particles for both 200 and 510 °C, indicating no wetting between the binder and the fine AlN particles. The spherical binder particles of size ≥ 10 μm had a smooth morphology at 200 °C and a rugged morphology at 510 °C, suggesting that the binder had different phases or compositions at different temperatures.

Fig. 7 shows an SEM photograph of the centre of an AlN preform with a binder/carrier ratio of 1:45. No binder was observed distinctly at either the centre or the edge of the preform. The resulting dry preform contained ~ 0.1 wt % binder.

Fig. 8 shows SEM micrographs at the centres of SiC and Al_2O_3 preforms which were prepared similarly as the AlN preforms. No binder was observed distinctly in either SiC or Al_2O_3 preforms. Like the AlN preform, the SiC preform exhibited no particle clustering. In contrast, the Al_2O_3 preform showed particle clustering throughout the preform, such that very fine particles were attached to the larger Al_2O_3 particles. As shown in the top right and left regions of Fig. 8b, little empty space was found due to the particle agglomeration. Such clustering caused Al/Al_2O_3 composites more difficulty for complete infiltration and resulted in inferior mechanical properties compared to Al/AlN and Al/SiC composites.

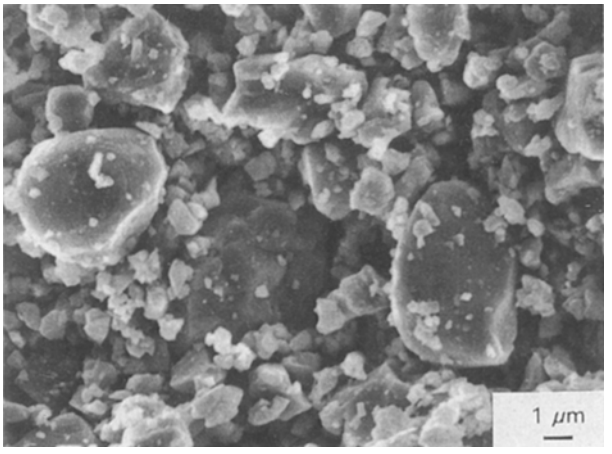

Figure 7 SEM micrograph of an AlN preform (in the centre region) fabricated with a carrier/binder ratio of 45:1 and baked at 510 °C.

2.5. Phases in preforms

A study of the reaction between the reinforcements, i.e. AlN, SiC or Al_2O_3, and the phosphate binder was accomplished by producing AlN, SiC or Al_2O_3 blocks (following [1–4]) with the undiluted phosphate binder solution, without any acetone addition. This means

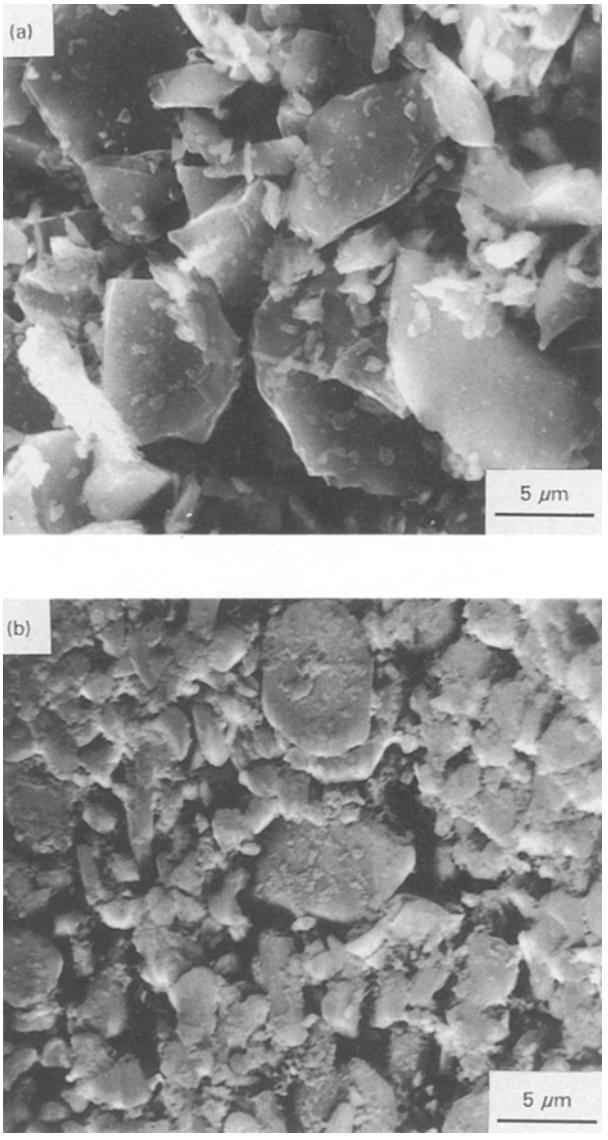

Figure 8 SEM micrographs of SiC and Al_2O_3 preforms (in the centre regions) fabricated with a carrier/binder ratio of 45:1 and baked at 510 °C. (a) SiC, (b) Al_2O_3.

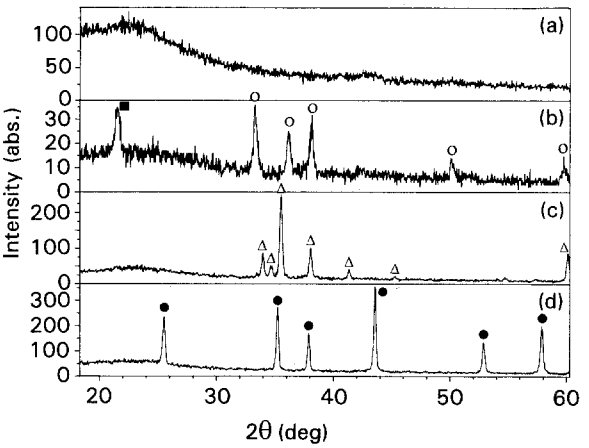

Figure 9 XRD patterns of the undiluted phosphate binder by itself and when mixed with AlN, SiC or Al_2O_3 powder at room temperature (without preform heating). ○, AlN; ■, $AlPO_4$ (cristobalite); △, SiC; ●, Al_2O_3.

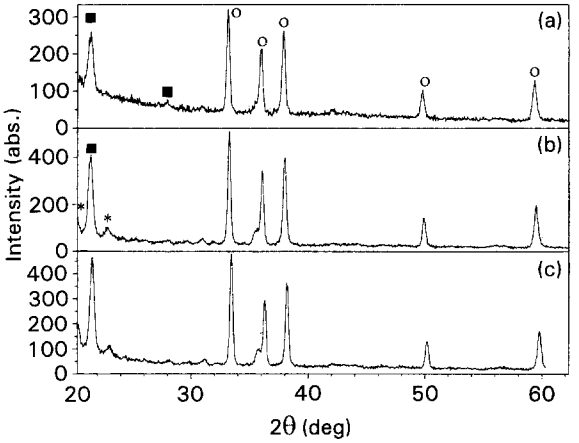

Figure 10 XRD patterns of AlN blocks made by using the undiluted phosphate binder and baked at (a) 200, (b) 510 and (c) 800 °C. ○, AlN; ■, $AlPO_4$ (cristobalite); *, $Al(PO_3)_3$ (B).

that the binder/carrier ratio was ∞. Although such blocks contained excess phosphate binder blocking the passage of infiltration and were not applicable to composite fabrication, their high binder content made the reinforcement/binder reaction experimentally more observable. The blocks were cylinders, 1.25 cm both in diameter and in height. Note that preforms prepared with binder/carrier ratios of 1/10 and 1/45 were 4.0 cm in diameter.

After mixing with the undiluted binder at room temperature, the AlN, SiC and Al_2O_3 mixtures were directly used for XRD study. Upon mixing at room temperature, AlN reacted with the undiluted binder and produced heat. The AlN mixture then became dried by its own heat, while the SiC and Al_2O_3 mixtures were still wet. Fig. 9 shows the XRD patterns of the undiluted binder and of the AlN, SiC and Al_2O_3 mixtures. The undiluted binder was amorphous at room temperature. For the AlN mixture, cristobalite aluminium orthophosphate ($AlPO_4$) was observed at room temperature (no preform baking), indicating a reaction of AlN with the undiluted binder. For SiC and Al_2O_3, no reaction was observed.

Fig. 10 shows the XRD patterns of the AlN blocks made with the undiluted phosphate binder and baked in air at 200, 510 and 800 °C. When the AlN blocks were dried in air at room temperature, they expanded due to the gas reaction product (presumably NH_3 or phosphorous gas), indicating a reaction between AlN and the phosphate binder. Upon mixing to form the block, the AlN reacted with the phosphate binder and released heat. No such expansion was observed for the SiC or Al_2O_3 blocks or for the AlN preforms prepared with a binder/carrier ratio of 1/10 or 1/45. The cristobalite $AlPO_4$ was formed due to the reaction between AlN and the phosphate binder at room temperature during mixing. At 200, 510 and 800 °C, the main reaction product was also cristobalite $AlPO_4$. In addition, a small amount of type-B aluminium metaphosphate ($Al(PO_3)_3$) formed in the blocks baked at 510 and 800 °C. The amount of cristobalite $AlPO_4$ increased with increasing baking temperature.

Fig. 11 shows the XRD patterns of the SiC blocks similarly prepared and baked in air at 200, 510 and 800 °C. It shows that a small amount of reaction

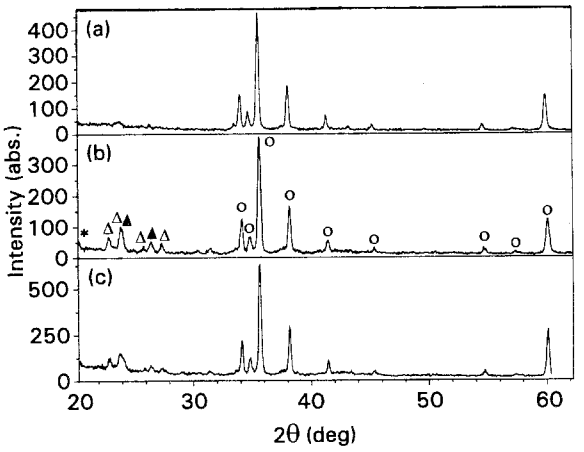

Figure 11 XRD patterns of SiC blocks made by using the undiluted phosphate binder and baked at (a) 200, (b) 510 and (c) 800 °C. ○, SiC; △, SiP_2O_7 (15–564); ▲, SiP_2O_7 (15–563); *, $Al(PO_3)_3$ (B).

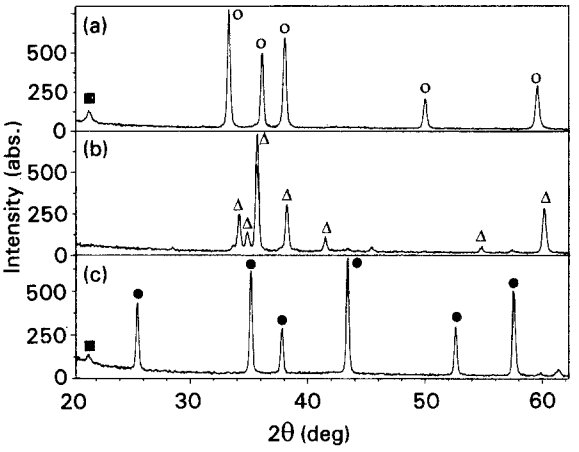

Figure 13 XRD patterns of (a) AlN, (b) SiC and (c) Al_2O_3 preforms (at the edge) fabricated with a carrier/binder ratio of 10:1 and baked at 510 °C. ○, AlN; ■, $AlPO_4$ (cristobalite); △, SiC; ●, Al_2O_3.

product was formed in the block baked at 200 °C. Two forms of silicon phosphate (SiP_2O_7) were formed from the reaction of SiC with the phosphate binder for the SiC blocks heated at both 510 and 800 °C. The binder phase found for these two blocks was type-B aluminium metaphosphate ($Al(PO_3)_3$) (Fig. 11). The SiC-phosphate binder reaction increased with increasing baking temperature from 200 to 510 °C and then did not change up to 800 °C.

Fig. 12 shows the XRD patterns of the Al_2O_3 blocks similarly prepared and baked in air at 200, 510 and 800 °C. It shows that at 200 °C, berlinite aluminium orthophosphate ($AlPO_4$) was dominant, together with a small amount of cristobalite aluminium orthophosphate ($AlPO_4$). Both berlinite and cristobalite $AlPO_4$ were probably formed due to the reaction between Al_2O_3 and the phosphate binder. The amount of cristobalite $AlPO_4$ increased at the expense of berlinite $AlPO_4$ with increasing baking temperature up to 800 °C. At 800 °C, no berlinite $AlPO_4$ was observed. Type B aluminium metaphosphate ($Al(PO_3)_3$) was present in the blocks baked at 800 °C.

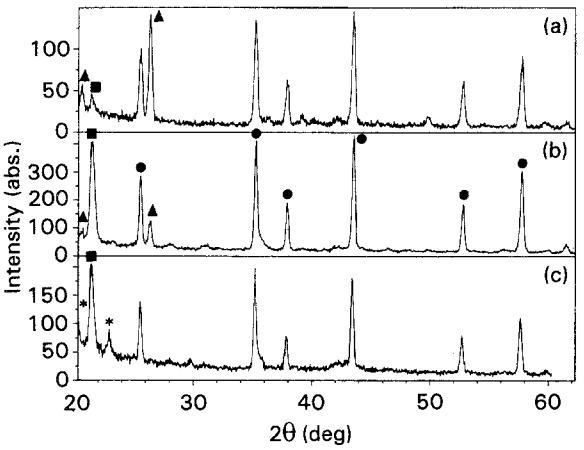

Figure 12 XRD patterns of Al_2O_3 blocks made by using the undiluted phosphate binder and baked at (a) 200, (b) 510 and (c) 800 °C. ▲, $AlPO_4$ (berlinite); ■, $AlPO_4$ (cristobalite); ●, Al_2O_3; *, $Al(PO_3)_3$ (B).

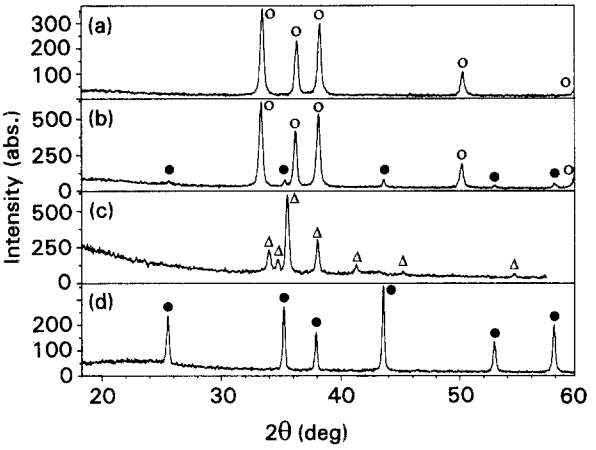

Figure 14 XRD patterns of AlN, SiC and Al_2O_3 preforms (at the edge) fabricated with a carrier/binder ratio of 45:1 and baked under various conditions. (a) AlN preform baked at 660 °C for 43 h. (b) A mixture of AlN and Al_2O_3 particles (1 wt %) showing clear Al_2O_3 X-ray diffraction peaks. (c) SiC preform baked at 510 °C for 8 h. (d) Al_2O_3 preform baked at 510 °C for 8 h. ○, AlN; △, SiC; ●, Al_2O_3.

Fig. 13 shows XRD patterns of AlN, SiC and Al_2O_3 preforms baked at 510 °C for 3 h. The carrier/binder ratio was 10:1. Both AlN and Al_2O_3 preforms showed a small amount of cristobalite $AlPO_4$ as the reaction product of the phosphate binder with either AlN or Al_2O_3. The amount of reaction product was limited as less phosphate binder was used compared to the case of the undiluted binder (binder/carrier ratio of ∞). No reaction product peak was found in the SiC preform due to less reactivity between the phosphate binder and SiC than between the binder and either AlN or Al_2O_3.

Fig. 14 shows XRD patterns of AlN, SiC and Al_2O_3 preforms heated at various conditions. No binder peak was observed, as the amount of binder in the preforms was too small to be detected.

2.6. Compressive strength of preforms

Compression testing was performed to determine the binding ability of the binder for AlN, SiC and Al_2O_3

preforms. The preforms were 0.5 in diameter and in height. Table IV shows the compressive strength of AlN preforms made by using the phosphate binder at various binder/carrier ratios and baked in air at 510 °C. The AlN preforms made with a binder/carrier ratio of 1/10 exhibited the highest compressive strength, whereas the AlN preforms made with undiluted binder (binder/carrier ratio of 1/0) showed the lowest compressive strength. As described in the previous section, the AlN reacted with the undiluted binder and resulted in gaseous porosity in the AlN preforms, so a binder/carrier ratio of 1/0 gave the lowest compressive strength. All AlN preforms made with various binder/carrier ratios exhibited shear cracks around the cylindrical edge. Although the AlN preform made with a binder/carrier ratio of 1/10 had a higher compressive strength compared to that made with a binder/carrier ratio of 1/45, it could not be used for composite fabrication. The excess binder in the AlN preform blocked the infiltration passage (especially at the cylindrical edge where the presence of binder was distinctly observed) and resulted in incomplete infiltration or even non-infiltration for AlN preforms made with a binder/carrier ratio of 1/10.

Table V shows the compressive strength of AlN, SiC and Al_2O_3 preforms made with a binder/carrier ratio of 1/45 and baked at 510 °C for 3 h. The Al_2O_3 preform exhibited the highest compressive strength, indicating the largest binding strength between the phosphate binder and Al_2O_3. On the other hand, the SiC preforms showed the lowest compressive strength. As shown in Fig. 13, less reaction occurred between SiC and the binder at 510 °C compared to that between either AlN or Al_2O_3 and the binder.

2.7. Thermal conductivity of preforms

Laser-flash thermal diffusivity testing was performed to determine the effect of baking conditions on the thermal conductivity of AlN, SiC and Al_2O_3 preforms. The thermal diffusivity was measured using a laser-flash thermal diffusivity analyser and the specific heat was measured using a differential scanning calorimeter (Perkin-Elmer DSC7). The thermal conductivity of AlN, SiC and Al_2O_3 preforms were obtained by multiplying together the preform density, the specific heat and the thermal diffusivity. Two baking conditions were considered: in air or in vacuum. The preforms were 0.5 inch in diameter and 0.20–0.25 inch in height. The preforms were made with a binder/carrier ratio of 1/45 and were baked at 510 °C in air or in vacuum ($\sim 10^{-3}$ torr). All preforms were coated on both surfaces with a thin layer of gold and subsequently a thin layer of carbon for good thermal measurements.

As shown in Table VI, AlN preforms exhibited the highest thermal conductivity, followed by Al_2O_3 preforms, and SiC preforms exhibited the lowest thermal conductivity. The Al_2O_3 preform had a higher thermal conductivity than the SiC preform due to its much higher volume fraction (i.e. a denser structure). The thermal conductivity of AlN and SiC preforms were slightly increased by baking in vacuum instead of baking in air, whereas the thermal conductivity of the Al_2O_3 preform was not affected by the baking environment. This is consistent with the fact that AlN and SiC can be oxidized to form less conductive Al_2O_3 and SiO_2, respectively, whereas Al_2O_3 cannot be further oxidized.

As shown in Table VII, all preforms had measured thermal conductivities which were much lower than those of the corresponding reinforcements (in their fully densified state) or the calculated values based on the ROM parallel model, but higher than the calculated values based on the ROM series model. The ROM parallel and series models were basically suitable for describing the thermal conductivity of continuous fibre composites in longitudinal and transverse directions, respectively. The measured thermal conductivity of each reinforcement preform was expected to be lower than the ROM parallel prediction, as the continuous phase (i.e. air) in the preform was

TABLE IV Effect of the binder/acetone ratio on the compressive strength of the AlN preforms baked at 510 °C for 3 h

Binder/acetone ratio	AlN volume fraction	Compressive strength (MPa)	Fracture mode
1/0	~ 0.27[a]	4.18 (0.73)	Shear cracks
1/10	~ 0.55	8.19 (1.33)	Shear cracks
1/45	~ 0.55	5.12 (0.76)	Shear cracks

Shown in parentheses are the standard deviations.
[a] Preform expanded due to the AlN–phosphate binder reaction.

TABLE V The compressive strength and calculated binder amount of AlN, SiC and Al_2O_3 preforms fabricated with a carrier/binder ratio 45:1 and baked at 510 °C for 3 h

Reinforcement	Volume fraction (%)	Compressive strength (MPa)	Binder amount (wt %)
AlN	55	5.12 (0.76)	0.1
SiC	55	3.83 (0.36)	0.1
Al_2O_3	60	10.43 (1.47)	0.1

TABLE VI The room temperature specific heat, thermal diffusivity and thermal conductivity[a] of AlN, SiC and Al_2O_3 preforms

Filler	Baking condition	Volume fraction	Density ($g\,cm^{-3}$)	Specific heat ($J\,g^{-1}\,°C$)	Thermal diffusivity ($mm^2\,s^{-1}$)	Thermal conductivity ($W\,m^{-1}\,°C$)
AlN	In air	0.535	1.744 (0.042)	0.846 (0.027)	1.08 (0.05)	1.60 (0.16)
	In vacuum	0.575	1.875 (0.014)	0.827 (0.032)	1.13 (0.13)	1.75 (0.28)
SiC	In air	0.495	1.590 (0.026)	0.734 (0.010)	0.56 (0.02)	0.65 (0.04)
	In vacuum	0.506	1.623 (0.021)	0.746 (0.025)	0.59 (0.06)	0.71 (0.11)
Al_2O_3	In air	0.617	2.454 (0.010)	0.842 (0.040)	0.55 (0.08)	1.14 (0.22)
	In vacuum	0.619	2.453 (0.041)	0.852 (0.012)	0.53 (0.06)	1.11 (0.16)

[a] Standard deviation shown in parentheses.

TABLE VII Comparison of the measured thermal conductivities of AlN, SiC and Al_2O_3 preforms with the theoretical predictions[a]

Filler	Volume fraction	Measured thermal conductivity[b] ($W\,m^{-1}\,°C$)	ROM parallel model[c]	ROM series model[d]	Empirical geometric mean model[e]
Air	1.0	0.0262	–	–	–
AlN	1.0	163	–	–	–
SiC	1.0	90	–	–	–
Al_2O_3	1.0	20	–	–	–
AlN	0.535	1.60 (0.16)	87.2	0.056	2.8
SiC	0.495	0.65 (0.04)	44.6	0.052	1.5
Al_2O_3	0.617	1.14 (0.22)	12.35	0.068	1.6

[a] Preforms were baked in air at 510°C. The continuous phase was assumed to be air.
[b] Standard deviation shown in parentheses.
[c] ROM or Halpin–Tsai theoretical model, $K_c = K_f v_f + k_m (1 - v_f)$.
[d] Halpin–Tsai theoretical model, $1/K_c = v_f/K_f + (1 - v_f)/K_m$.
[e] Ratcliffe empirical model, $K_c = K_f^{vf} K_m^{vm}$.

thermally insulating. On the other hand, the ROM series model is valid only if the reinforcement particles were enclosed in air without any contact between the particles. The measured thermal conductivity was closest to the prediction of the geometrical mean empirical model [5] due to partial reinforcement contacts in the preform.

Although negligible improvement in preform thermal conductivity was achieved for each kind of reinforcement due to baking in vacuum, the thermal diffusivity of Al/AlN composites increased due to baking in vacuum (instead of air) at 510 °C or in air at 200 °C (instead of 510 °C). This indicates that a suitable preform baking environment or temperature diminishes the oxidation of the AlN particles and provides a cleaner reinforcement–matrix interface in the resulting composite. Since Al is more thermally conducting than AlN, a clean Al–AlN interface is important. The thermal conductivity of Al/AlN was improved by preform baking in vacuum, while that of Al/SiC was not; this is due to the superior oxidation resistance of SiC compared to AlN.

2.8. Composite fabrication

Pure aluminium (170.1) was used; its composition was 99.77% Al, 0.16% Fe and 0.07% Si, as supplied by Roth Bros. Smelting Corp. The melting temperature of Al is 660 °C.

The MMCs were fabricated by vacuum infiltration of a liquid metal into a porous preform under an argon pressure. The mould chamber was evacuated using a mechanical pump. A series of inert gas (argon) bottles were connected to the chamber with tubes and a valve. If the pressure of the inert gas in the bottle was lower than that in the chamber, a compressor had to be used to increase the chamber pressure when needed. The compressor was capable of pressurizing the mould chamber at a rate of 5.5 MPa min^{-1}.

The chamber wall was strong enough to allow simultaneously high pressure and temperature – at least 55.2 MPa and 800 °C. The inner wall surface of the mould chamber was coated with a graphite paste for ease of demoulding, if the mould was made of steel. The graphite paste was a mixture of graphite powder (G-67, Fisher Scientific Co., grade #38) and silica colloid (30% SiO_2 in water, EM Science SK0140-1). The graphite paste also prevented severe iron contamination of the aluminium alloy melt and composite by the steel mould. Thermocouples were in contact with the outer wall of the mould chamber – one near to the aluminium melt in the upper part and one near to the preform at the bottom of the mould chamber.

The mould chamber was heated using a graphite heating element. The temperature in any part of the chamber was approximately the same before liquid metal infiltration. However, after complete infiltration, the mould chamber was cooled so that the

temperature of the bottom part of the chamber was 40 °C lower than that of upper part of the chamber. This temperature difference ensured that the aluminium melt solidified upward from the bottom of the mould chamber. The aluminium melt also solidified radially inward from the mould surface.

The procedure used for the fabrication of MMCs is schematically illustrated in Fig. 15 for an infiltration temperature of 780 (± 20) °C. The entire procedure may be divided into seven steps, which are described below.

A_0–A_1 The preform was placed at the bottom of a steel mould. Above the preform was placed an aluminium ingot. The mould chamber was then sealed and evaculated to a pressure of 6.7 to 26.7 Pa.

A_1–A_2 The chamber and its loadings were superheated 100–150 °C above the liquidus temperature of the alloy, i.e. 800 °C for the infiltration temperature of 780 (± 20) °C. In the meantime, evaculation continued.

A_2–A_3 The temperature was maintained for a period to ensure that the alloy melted completely and that the temperature of any part of the chamber was approximately equal.

A_3–A_4 The temperature was allowed to drop at a rate of 3.0 to 10.0 °C min^{-1} to or near the liquidus temperature – in this case 670 °C. When the temperature just started to drop from 800 °C, argon gas was introduced to pressurize the mould chamber from 0 Pa to the infiltration pressure of 24, 31, 41 or 55 MPa. This pressure (called the infiltration pressure) was applied to the surface of the melt to force the melt to penetrate the porous preform completely (Fig. 14). The chamber temperature dropped to about 760 °C when the pressure reached 41 MPa. The average mould temperature of 780 (± 20) °C is considered the infiltration temperature. A time of 3–7 min was required to reach the infiltration pressure, depending on the value of the infiltration pressure.

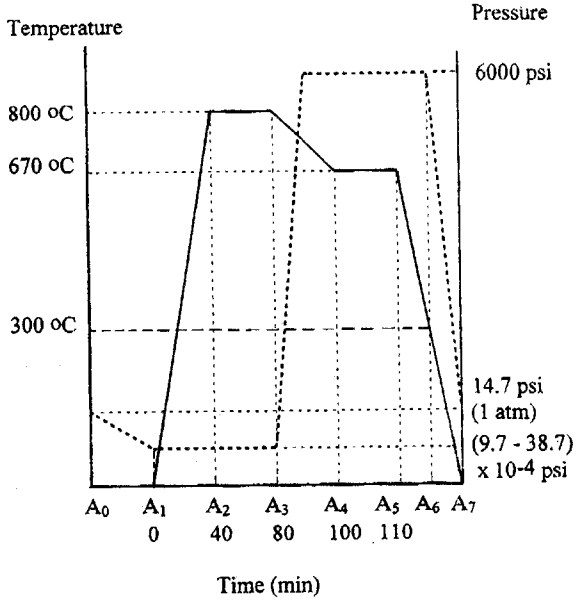

Figure 15 Schematic diagram of the temperature (——) and pressure (– – –) variations in the process of liquid metal infiltration.

A_4–A_5 The temperature and pressure of the chamber was maintained in this period to make sure that the infiltration of liquid aluminium into the preform was complete.

A_5–A_6 The chamber started cooling for the aluminium melt to solidify. In order to increase the cooling rate of the chamber, a cooling water jacket outside the chamber was used. The pressure was maintained during the solidification period. A lower temperature profile in the bottom region, compared to the top region, of the mould chamber resulted due to the use of the water jacket. This caused the aluminium melt to start solidification inward and upward from the circular edge and the bottom of the mould.

A_6–A_7 When the mould temperature reached 300 °C, the outlet valve was opened to release the inert gas. Premature release would result in shrinkage, and thus in cavities in the composite. The lid of the chamber was then opened, and the composite material was demoulded from the chamber.

The inert gas used was argon, due to its inertness and availability. Although nitrogen was lower in price and provided a beneficial effect to the infiltration of aluminium [6], it was not used. The nitrogen may react with the aluminium melt, especially in the presence of magnesium and silicon, to form aluminium nitride (AlN).

Unless stated otherwise, the infiltration temperature and pressure used were 780 (± 20) °C and 41 MPa for the fabrication of all composites.

2.9. Structure of composites

Fig. 16 shows optical micrographs of polished (not etched) sections of AlN composites prepared at infiltration pressures of 24, 31 and 41 MPa. The porosity decreased with increasing pressure: 12.4% at 24 MPa (Fig. 16a), 5.4% at 31 MPa (Fig. 16b), and 1.1–1.4% at 41 MPa (Fig. 16c) for a composite containing 58.6 vol % AlN. Fig. 16c, for the composite fabricated at 41 MPa represents one of the most thoroughly infiltrated composites in this work. A higher magnification SEM image of a similar composite containing 62.5% AlN is shown in Fig. 17; the porosity was 0.5%.

Fig. 18 shows an optical micrograph of a polished (not etched) section of a composite containing 60 vol % AlN, made with Al–5Mg as the matrix at an infiltration pressure of 24 MPa. The porosity was 2.7%. Thus, Mg in the matrix alloy enabled the required infiltration pressure to decrease to 24 MPa.

The Al/SiC composite fabricated at 41 MPa exhibited less porosity than the Al/AlN composite fabricated at the same pressure because of the superior wettability between Al and SiC. The superior wettability was due to the interfacial reaction of SiC with Al. It has been reported [7] that a 52% SiC particulate compact of 9.63 μm particle size could be infiltrated with pure aluminium at 800 °C and just 724 kPa.

As shown in Fig. 19, different microstructures (after mechanical polishing) were found between the cylindrical edge and body centre regions of the Al/SiC composite cylinder fabricated at an infiltration

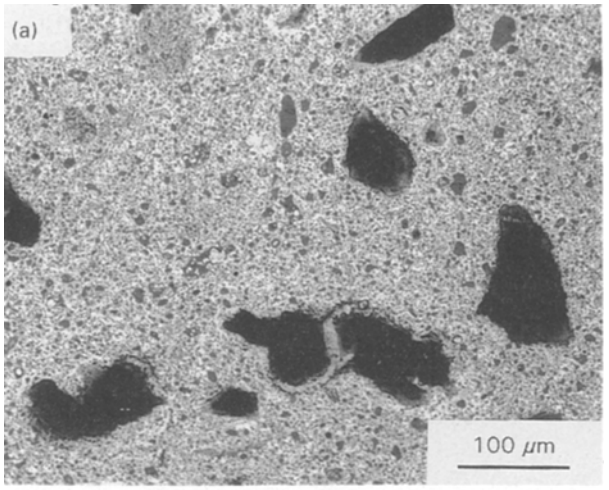

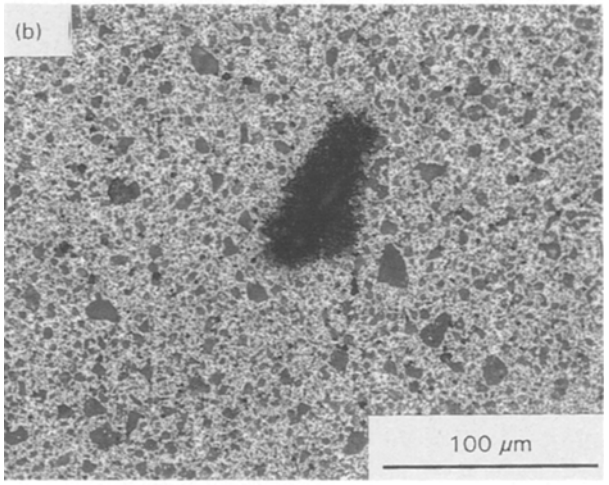

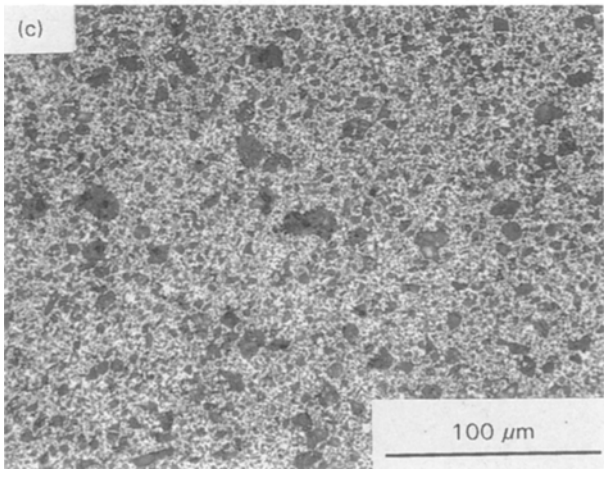

Figure 16 Optical micrographs (after mechanical polishing, without etching) of Al/AlN fabricated at an infiltration pressure of (a) 24, (b) 31 and (c) 41 MPa. Porosity decreased with increasing infiltration pressure.

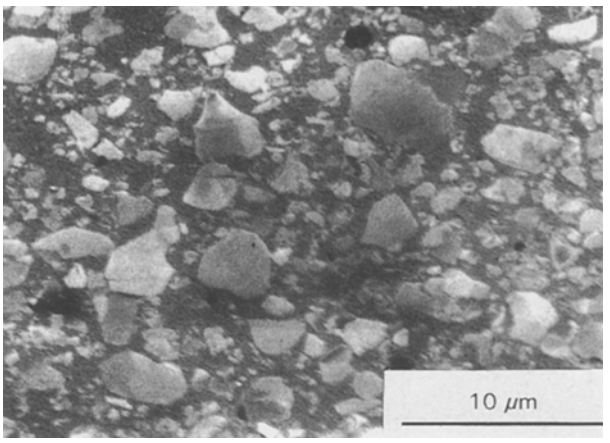

Figure 17 SEM micrograph of Al/AlN (62.5 vol % AlN) fabricated at an infiltration pressure of 41 MPa. Porosity, 0.5%.

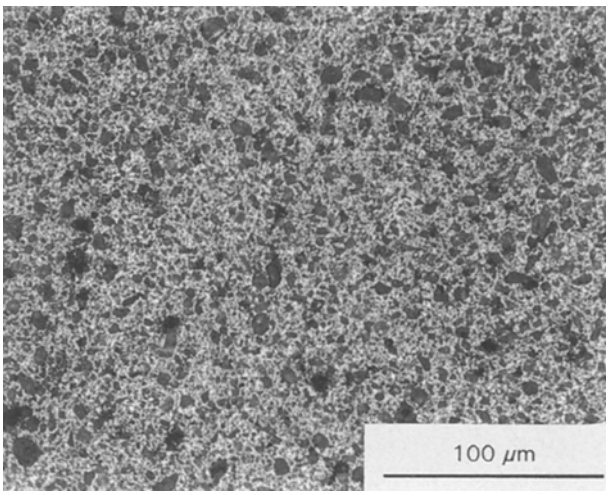

Figure 18 Optical micrographs (after mechanical polishing, without etching) of Al–5Mg/AlN fabricated at an infiltration pressure of 24 MPa.

temperature of 780 ($\pm$ 20) °C. The difference in microstructure is related to the more extensive interfacial reaction between Al and SiC in the edge region, which was next to the excess aluminium. More Al–SiC reaction occurred around the edge due to the proximity to the excess aluminium and a longer metal–particle contact time during infiltration. The edge region indeed showed a lower density of SiC particles than the centre region. On the other hand, the brittle reaction product weakened the Al/SiC interface, probably causing some SiC particles to be partly removed during polishing. As compared to Fig. 6 of [8] (which shows a reaction product non-uniformly lining the Al/SiC interface after heating at 997 °C for 1 h), the clear-cut outlines of SiC particles in the centre region (Fig. 19) is an indication of relatively little reaction between Al and SiC. In comparison, as shown in Fig. 19, the edge and central regions of Al/AlN composite cylinder (60 vol % AlN) show essentially no difference in microstructure.

Further evidence for the Al–SiC reaction is provided by the observation of silicon precipitates ($\sim$ 5 vol %) in the excess aluminium case around the composite cylinder. (This aluminium contained no preform.) Optical microscopy of a polished section (Fig. 20a) showed faceted Al–Fe–Si precipitates (about 100 μm in size) touching the edge and outside the edge of the Al/SiC composite. Smaller needle-shaped Si, binary Al–Fe and ternary Al–Fe–Si precipitates were also present non-uniformly in the grain boundaries of the excess aluminium cast farther away

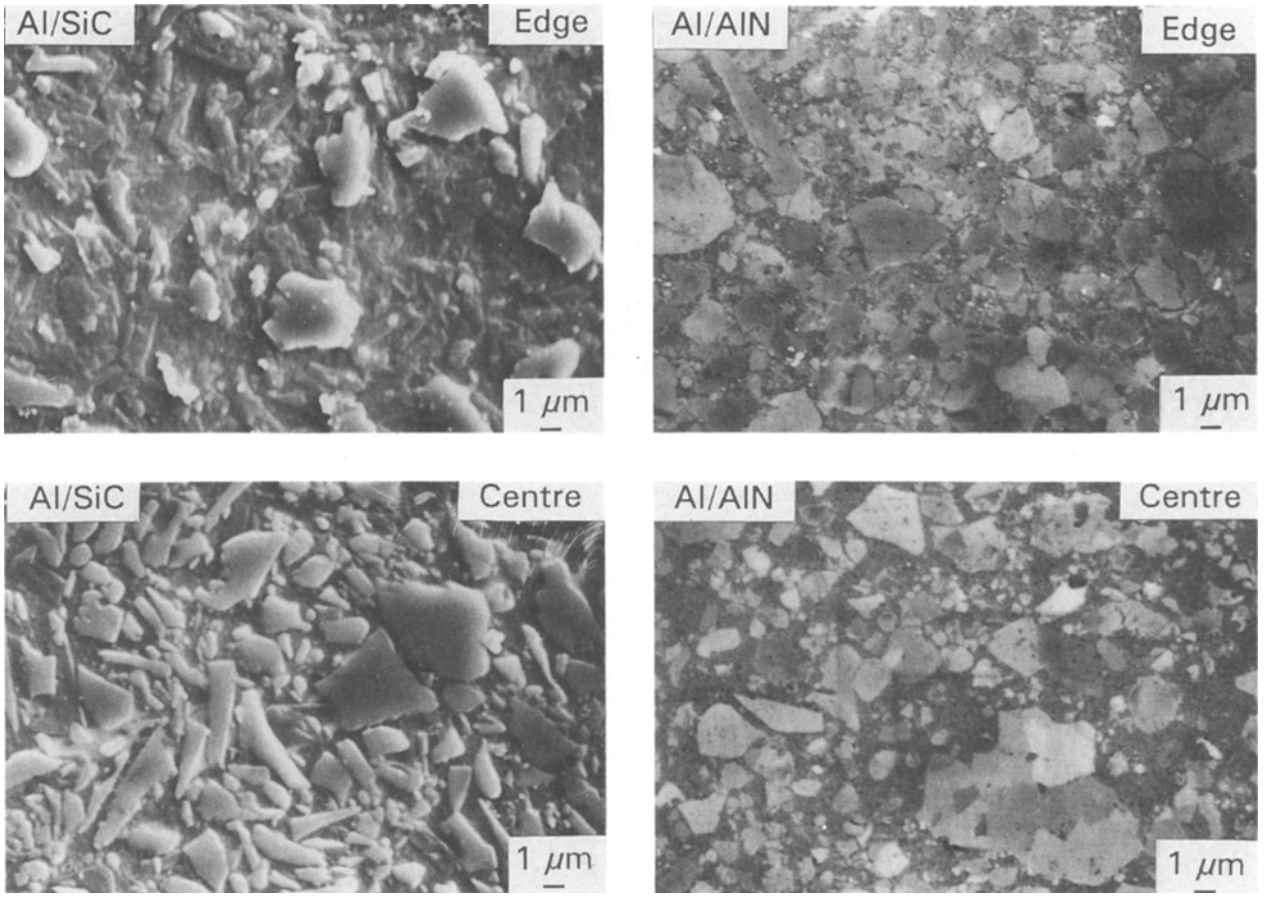

Figure 19 SEM micrographs (after mechanical polishing, without etching) of Al/AlN and Al/SiC in the edge and central regions of the composite cylinders.

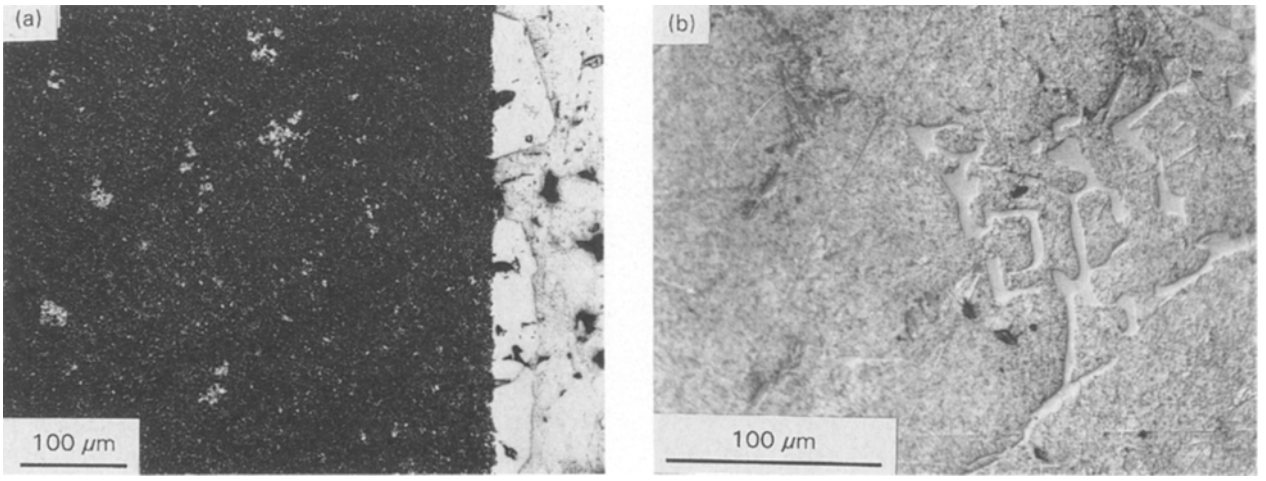

Figure 20 Optical microscope photographs of a polished section of the Al/SiC composite, showing (a) faceted ternary Al–Fe–Si precipitates (bright) touching the edge of the composite (dark) and residing in the excess aluminium region (the right 1/5 of the photographs), (b) needle-shaped and smaller ternary Al–Fe–Si, binary Al–Fe and Si precipitates in the excess aluminium region further away from the edge of the composite. (b) At a higher magnification than (a).

from the Al/SiC composite cylinder (Fig. 20b). The Si was the product of the reaction between Al and SiC. It was first formed in the edge region of the composite during infiltration and probably resulted in an Al–Si solution, which diffused outward into the surrounding Al melt. No Al–12Si eutectic or dendritic morphology was microscopically observed within the Al/SiC composite itself.

In contrast to Al/SiC, the Al/Al_2O_3 composites fabricated under the same conditions (41 MPa, 800 °C) showed more porosity than Al/AlN. Fig. 21a shows an optical micrograph of a polished (not

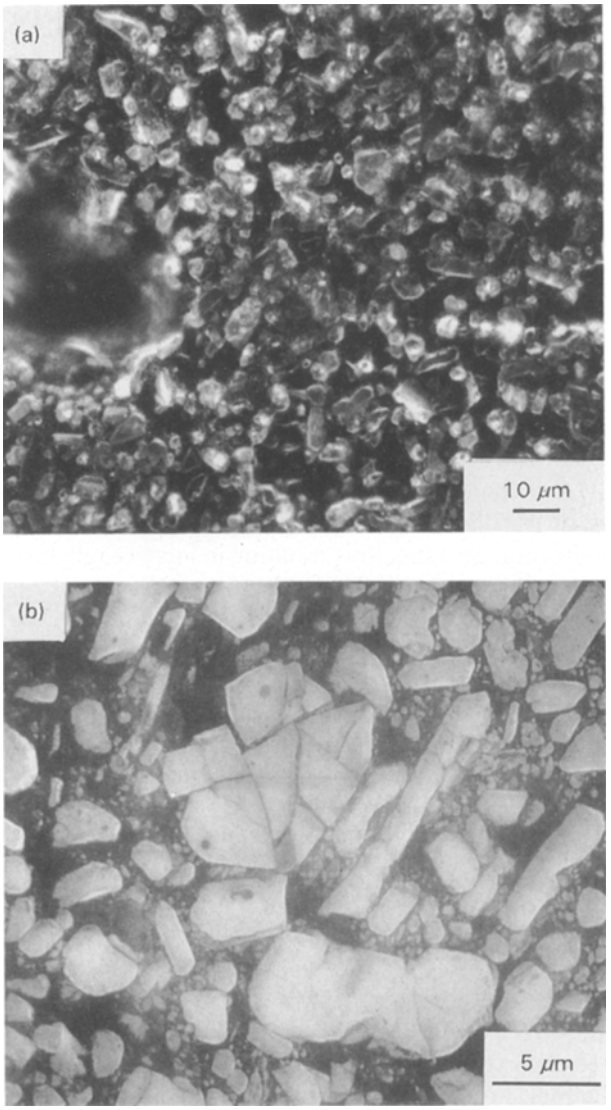

Figure 21 (a) Dark-field optical micrograph of Al/Al_2O_3 (61.4 vol % Al_2O_3), showing small (< 50 μm) but uniformly distributed pores throughout the composite. (b) SEM micrograph of the same composite. Particle cracking was readily observed in (b).

etched) Al/Al_2O_3 (61.4 vol % Al_2O_3) composite, in which small (< 50 μm) but uniformly distributed pores existed throughout the composite. These pores were Al_2O_3 powder aggregates which were not infiltrated and were therefore removed during specimen polishing in metallurgical sample preparation. Fig. 21b shows an SEM micrograph of the same sample in which Al_2O_3 particle cracks were readily observed, indicating a weaker particle strength for Al_2O_3. The porosity was 3 to 5%.

A similar morphology of pores was observed for the Al/Al_2O_3 composites fabricated at 41 MPa and 1000 °C, and at 55 MPa and 800 °C. This indicates that increasing either the infiltration temperature to 1000 °C or the infiltration pressure to 55 MPa could not further facilitate aluminium infiltration into the Al_2O_3 preform.

2.10. Mechanical properties of composites

Tensile testing was performed using a hydraulic mechanical testing system. The loading rate was 534 N min^{-1}. Dogbone-shaped specimens were obtained by cutting the as-cast composite cylinder parallel to the cylindrical axis to form two plates, which were then double-side grooved to the required dimension, as shown in Fig. 22a. The dimensions of the specimens are shown in Fig. 22b. The Young's modulus was measured using a strain gauge at low loads.

Typical stress–strain curves of Al/AlN, Al/SiC, Al/Al_2O_3 and pure Al are shown in Fig. 23. In contrast to the ductile Al matrix, all Al/AlN, Al/SiC and Al/Al_2O_3 composites exhibited failure strains less than 1.0%. Table VIII shows the tensile properties at room temperature of Al/AlN, Al/SiC and Al/Al_2O_3

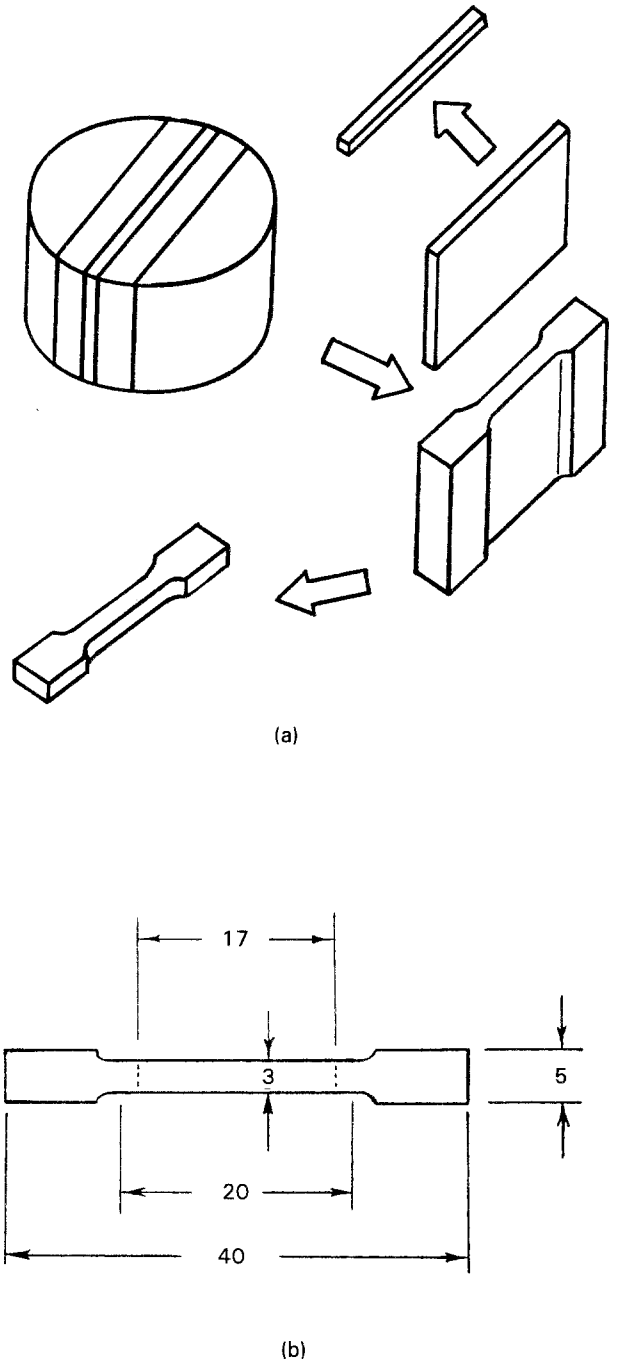

Figure 22 (a) In a composite cylinder, the central slab was used for X-ray diffraction investigation, while the two adjacent slabs were machined into the dog-bone shape for tensile test samples. (b) Specimen geometry for tensile testing. Numbers shown are dimensions in mm; dashed lines indicate gauge length markings on the specimen.

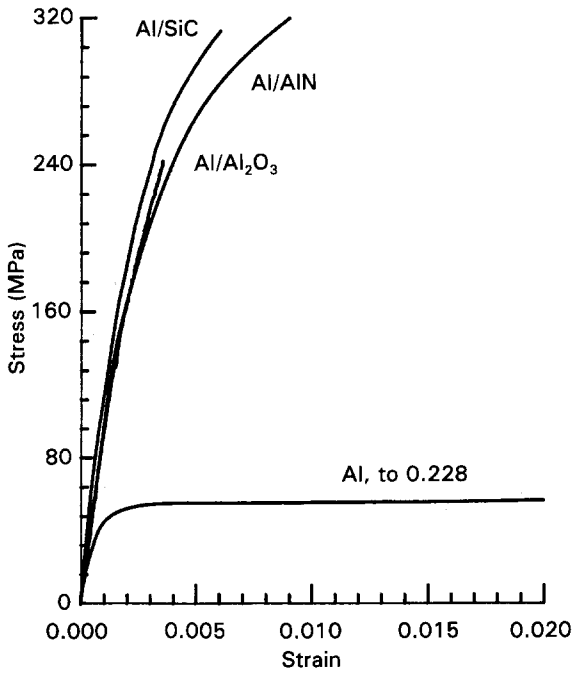

Figure 23 Typical stress–strain curves of Al/AlN, Al/SiC, Al/Al_2O_3 and pure aluminium.

composites. The strength and modulus were much increased and the ductility much decreased by the addition of AlN, SiC or Al_2O_3. Al/AlN and Al/SiC of similar reinforcement volume fractions (2nd and 3rd rows of Table VIII) exhibited similar tensile strengths, but the ductility was slightly higher for Al/AlN than Al/SiC. Comparison of Al/AlN and Al/Al_2O_3 of similar reinforcement volume fractions (4th and 5th rows of Table VIII) showed that Al/AlN had much higher strength and ductility than Al/Al_2O_3. For both Al/AlN and Al/Al_2O_3, the measured modulus and that calculated using the model of Hashin & Shtrikman [9] agree well with each other, but Al/SiC had a measured modulus which was larger than the theoretical value based on this model. This may be ascribed to the large aspect ratio (> 3 based on Fig. 19) of the SiC particles – a factor which was not considered in the Haslin & Shtrikman model. In contrast, the AlN and Al_2O_3 particles were equiaxed (aspect ratio = 1). Among the three kinds of reinforcement, Al/Al_2O_3 exhibited the lowest tensile properties due to particle clustering in the preform and incomplete liquid metal infiltration during composite fabrication.

Fig. 24 shows the tensile properties and porosity of Al/AlN (59–60 vol % AlN) fabricated at infiltration pressures of 24, 31, 41 and 55 MPa. The modulus, strength and ductility of Al/AlN increased with increasing infiltration pressure up to 41 MPa and remained essentially unchanged upon further increase in pressure. Note that the strength and ductility of Al/AlN increased linearly with increasing infiltration pressure up to 41 MPa. The modulus and strength of Al/AlN fabricated at an infiltration pressure of 55 MPa were similar to or slightly higher than those of Al/AlN fabricated at an infiltration pressure of 41 MPa is an optimum pressure for making sound Al/AlN composites. As shown in Fig. 24d, the porosity of Al/AlN composites decreased with increasing infiltration pressure, thus resulting in increasingly better tensile properties. The infiltration pressures of 24, 31 and 41 MPa yielded composites containing 12.4, 54.0 and 1.1 $\sim$ 1.4% porosity, respectively.

Table IX shows the tensile properties of Al/AlN composites, the preforms of which had been heat-treated under various conditions. The tensile strength of Al/AlN may be unchanged or slightly increased due to preform baking either in air at 200 °C or in vacuum at 510 °C, while the modulus and ductility were not affected by the baking conditions. The slight increase in tensile strength may be due to a cleaner and stronger Al–AlN interface.

Room temperature tensile fracture surfaces are shown in Fig. 25 for Al/AlN (58.6 vol % AlN) and Al/SiC (55.0 vol % SiC). Both fracture surfaces exhibited cleavage surfaces of the filler particles and microdimples in the Al matrix, but the proportion of cleavage surfaces is lower in Al/AlN than in Al/SiC, indicating higher ductility in Al/AlN. Moreover, no particle pull-out was observed in Al/AlN whereas particle pull-out was observed in Al/SiC, as shown by the SiC particle ($\sim$ 5 μm in size) located in the lower half of the Al/SiC photograph in Fig. 25. This indicates stronger bonding between Al and AlN than between Al and SiC. Note the presence of typical serratic fracture surfaces in the SiC particles in Fig. 25. In contrast, Al/Al_2O_3 exhibited fewer but coarser microdimples and little particle cleavage (Fig. 26). Small clusters of Al_2O_3 particles without being infiltrated

TABLE VIII Room temperature tensile properties[a] of Al/AlN, Al/SiC and Al/Al_2O_3 composites

Volume fraction	Strength (MPa)	Modulus (GPa)		Ductility (%)
		Measured	Theoretical[b]	
0	72.7 (1.1)	61.7 (3.4)	–	22.8 (1.9)
55.0% SiC	313.0 (37.5)	183.4 (15.0)	158.5	0.7 (0.3)
58.6% AlN	300.9 (25.2)	144.3 (4.2)	146.7	1.1 (0.4)
63.3% AlN	406.3 (33.9)	163.5 (6.5)	159.4	1.0 (0.2)
61.2% Al_2O_3	275.8 (14.6)	161.6 (6.9)	158.9	0.5 (0.1)
70.2% Al_2O_3	237.8 (8.4)	181.4 (10.8)	187.8	0.4 (0.1)

[a] Standard deviation shown in parentheses.
[b] Hashin & Shtrikman [9].
E_{AlN} = 345 GPa, E_{SiC} = 440 GPa, $E_{Al_2O_3}$ = 379 GPa.

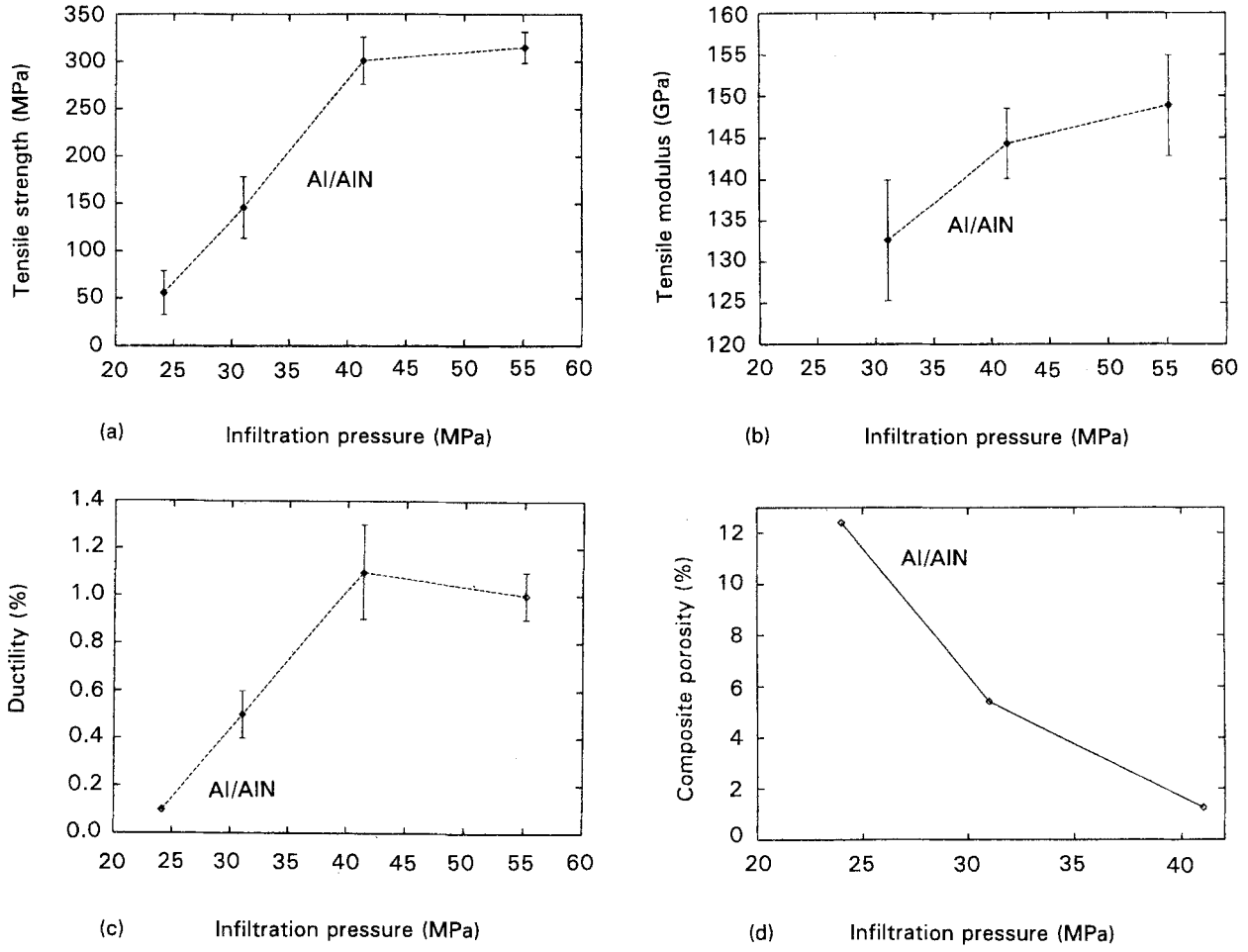

Figure 24 Tensile properties and porosity of Al/AlN (59–60 vol % AlN) and Al–5Mg/AlN (60 vol % AlN) as a function of the infiltration pressure. (a) Tensile strength, (b) modulus, (c) ductility, (d) porosity.

TABLE IX Effect of preform baking conditions on the room temperature tensile properties[a] of Al/AlN composites

Volume fraction	Preform baking condition	Strength (MPa)	Modulus (GPa)	Ductility (%)
58.6% AlN	510 °C, in air	300.9 (25.2)	144.3 (4.2)	1.1 (0.4)
58.0% AlN	510 °C, in vacuum	353.5 (57.3)	144.0 (13.4)	0.9 (0.3)
59.0% AlN	200 °C, in air	331.8 (23.8)	147.7 (6.2)	1.0 (0.1)

[a] Standard deviation shown in parentheses.

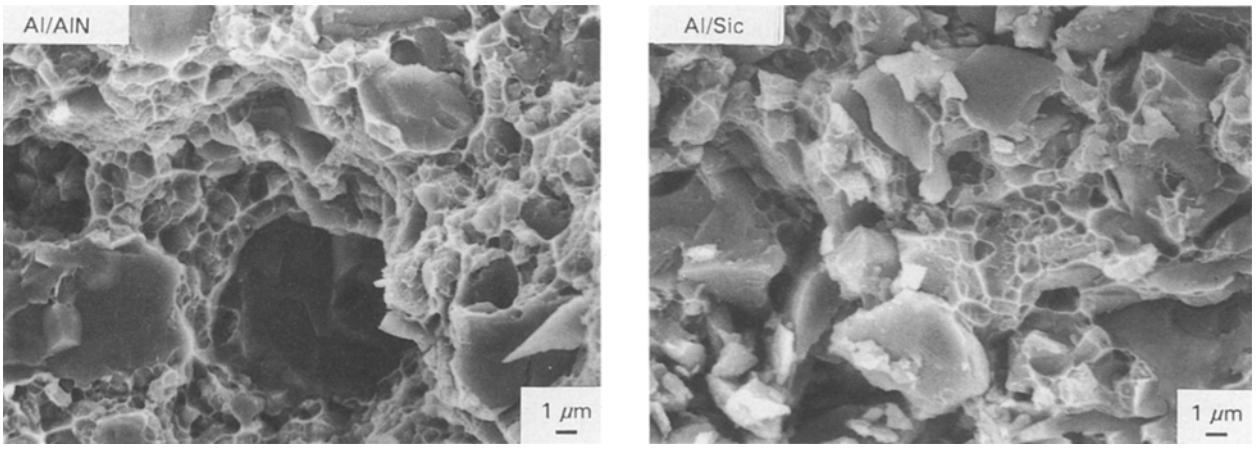

Figure 25 SEM micrographs of the tensile fracture surfaces of Al/AlN (58.6 vol % AlN) and Al/SiC (55.0 vol % SiC) tested at room temperature.

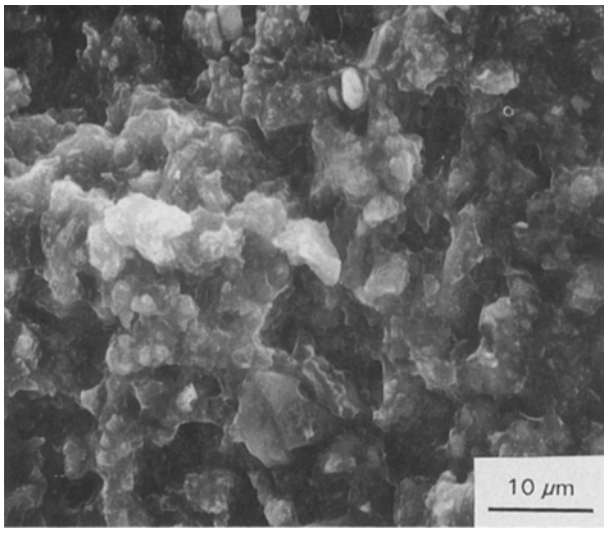

Figure 26 SEM micrograph of the tensile fracture surface of Al/Al_2O_3 (61.4 vol % Al_2O_3) tested at room temperature.

were observed on the fractured surface, and resulted in a poor tensile strength. Small pores were also observed on the fraction surface.

2.11. Thermal conductivity of composites

Both the thermal diffusivity and the specific heat of Al, Al/AlN and Al/SiC were measured in order to obtain their thermal conductivities. In order to find the optimum thermal diffusivity, the measured thermal diffusivity was obtained by utilizing an iterative procedure. Fig. 27a shows a typical data set of temperature rise against time for an Al/AlN composite (60 vol % AlN); a theoretical straight-line fit for the optimum thermal diffusivity for the corresponding data set is shown in Fig. 27b. The specific heat was measured by differential scanning calorimetry (Perkin-Elmer DSC7) using a Saffire reference. Table X shows the measured density, specific heat, thermal diffusivity and the resulting thermal conductivity of Al (170.1), AlN substrate, SiC substrate, Al/AlN (various AlN volume fractions), and Al/SiC (55 vol % SiC). The preforms of such composites were baked in air. The thermal diffusivity and conductivity of AlN composites decreased with increasing volume fraction of the reinforcement. The AlN composites had higher thermal conductivities than SiC composites, even though the filler volume fraction was higher in Al/AlN than Al/SiC. This implies that Al/AlN had a larger thermal conductivity than Al/SiC of the same filler volume fraction.

As also shown in Table X, AlN composites, the preforms of which were baked in air at 510 °C, exhibited lower thermal diffusivities than those with the preforms baked in vacuum at 510 °C or in air at 200 °C. This is due to the oxide or oxynitride layer on the AlN particles. As confirmed by thermogravimetric analysis, oxidation of AlN occurred in air at 500 °C, but essentially not at 200 °C (See Appendix 1). The oxide or oxynitride layer prevented an intimate interface between Al and AlN, thus resulting in a lower

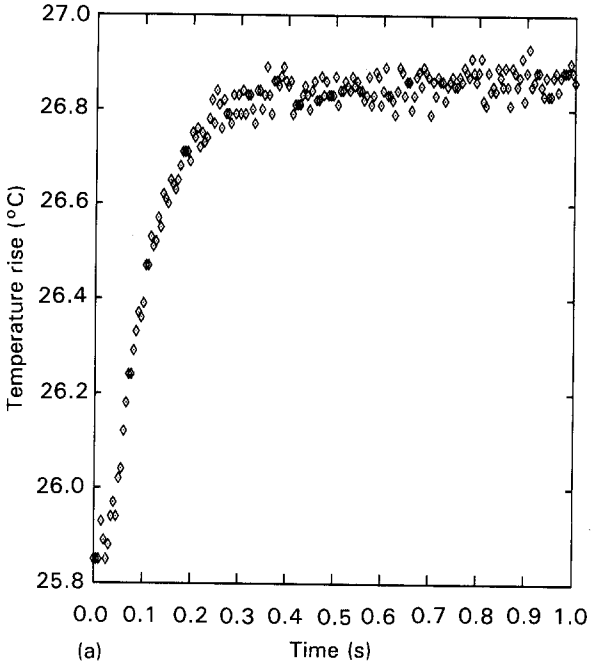

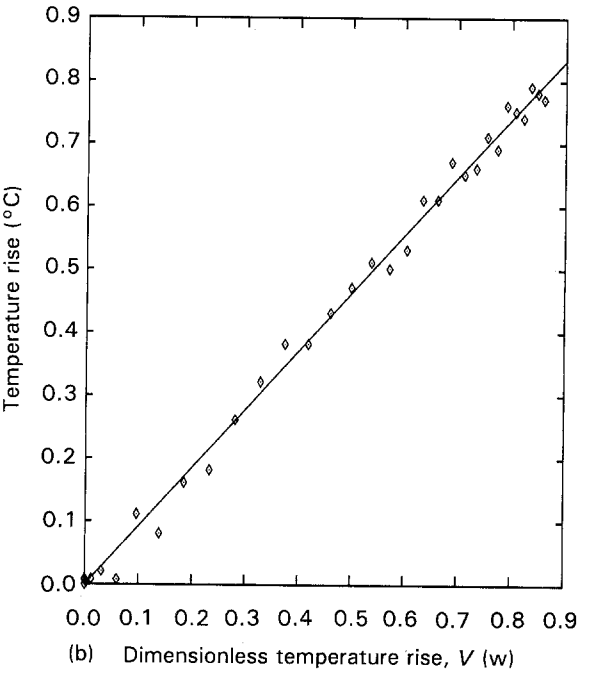

Figure 27 (a) Typical data set of thermocouple temperature rise against time for an Al/AlN composite (60 vol % AlN). (b) Straight-line theoretical fit for the optimum thermal diffusivity of (a). $a = 52.46 \times 10^{-6}\ m^2\ s^{-1}$.

thermal diffusivity for the Al/AlN composite. In contrast, the Al/SiC composite exhibited essentially no increase in thermal conductivity as the SiC preform was baked in vacuum (instead of air). However, no improvement in thermal conductivity was observed for both AlN and SiC preforms (not composite) baked in vacuum.

3. Discussion

3.1. Effect of binder-reinforcement reactivity

The phosphate binder was found to be reactive with AlN, SiC and Al_2O_3 powders. Table XI summarizes

TABLE X Room temperature specific heat, thermal diffusivity and thermal conductivity of Al/AlN and Al/SiC composites, as well as pure Al, pure AlN and pure SiC[a]

Material	Density ($g\,cm^{-3}$)	Specific heat ($J\,g^{-1}\,°C$)	Thermal diffusivity ($mm^2\,s^{-1}$)	Thermal conductivity ($W\,m^{-1}\,°C$)
Al	2.697	0.92595 (± 0.0019)	84.7 (2.4)[b]	211.8 (6.4)
AlN[c]	3.236	0.75968 (± 0.0038)	65.4 (2.3)	160.7 (6.4)
SiC[d]	3.103	0.70704 (± 0.0184)	54.0 (2.1)	118.5 (7.7)
60.0 vol % AlN	3.036	0.81866 (± 0.0643)	53.8 (1.2)	133.7 (13.5)
62.7 vol % AlN	3.019	0.81332 (± 0.0400)	52.6 (0.9)	129.2 (8.6)
64.6 vol % AlN	3.062	0.81800 (± 0.0005)	51.4 (1.5)	128.7 (3.8)
55.0 vol % SiC	2.979	0.80486 (± 0.0025)	52.4 (2.9)	125.6 (3.1)
58.0 vol % AlN (in vacuum[e], 510 °C)	2.992	0.84241 (± 0.0138)	62.7 (1.4)	158.0 (6.1)
59.0 vol % AlN (in air, 200 °C)	3.016	0.83730 (± 0.0287)	62.1 (2.3)	156.9 (11.2)
55.0 vol % SiC (in vacuum[e], 510 °C)	2.959	0.81910 (± 0.0063)	53.7 (2.7)	130.2 (7.5)

[a] Unless stated otherwise, the preforms were baked in air at 510 °C.
[b] Standard deviation shown in parentheses.
[c] AlN substrates obtained from Advanced Refractory Technologies, Inc.
[d] SiC substrates obtained from Carborundum Company.
[e] $\sim 10^{-3}$ torr.

TABLE XI Summary of binder and reaction product phases in AlN, SiC and Al_2O_3 blocks fabricated with binder/carrier ratio of 1:10 and baked at various temperatures

Baking temperature (°C)	AlN block[a]	SiC block	Al_2O_3 block	Undiluted binder (no reinforcement)
25	Strong reaction RP: $AlPO_4$ (Cr) BP: none	No reaction RP: none BP: none	No reaction RP: none BP: none	–
200	RP: $AlPO_4$ (Cr) BP: none	RP: none BP: none	RP: $AlPO_4$ (Ber), $AlPO_4$ (Cr) BP: none	BP: $Al(PO_3)_3$ (A + B)
510	RP: $AlPO_4$ (Cr) BP: $Al(PO_3)_3$ (B)	RP: SiP_2O_7 BP: none	RP: $AlPO_4$ (Cr), $AlPO_4$ (Ber) BP: $Al(PO_3)_3$ (B)	BP: $Al(PO_3)_3$ (A + B)
800	RP: $AlPO_4$ (Cr) BP: $Al(PO_3)_3$ (B)	RP: SiP_2O_7 BP: none	RP: $AlPO_4$ (Cr), $AlPO_4$ (Ber) BP: $Al(PO_3)_3$ (B)	BP: $Al(PO_3)_3$ (A)

[a] RP, reaction product; BP, binder phase; Cr, Cristobalite; Ber, Berlinite.

the presence or absence of reaction and the associated reaction product phase in various preforms at various temperatures. At room temperature, the phosphate binder strongly reacted with AlN. No reaction between phosphate and SiC or Al_2O_3 was observed at room temperature. For the case of AlN, the reaction product was cristobalite $AlPO_4$ at room temperature and various heating temperatures. The binder phase in AlN preform was $Al(PO_3)_3$ (B), which existed only at 510 and 800 °C (not at 200 or 25 °C). For the case of SiC, no reaction product or binder phase was observed at 25 or 200 °C. At 510 or 800 °C, the reaction product silicon phosphate, SiP_2O_7, was dominant, with no binder phase observed. No reaction between the binder and Al_2O_3 was observed at room temperature. However, the reaction occurred at 200 °C or above to form predominantly berlinite $AlPO_4$ and cristobalite $AlPO_4$. The amount of cristobalite $AlPO_4$ increased, at the expense of berlinite $AlPO_4$, with increasing baking temperature. The binder phase at 510 and 800 °C was $Al(PO_3)_3$ (B).

Although $Al(PO_3)_3$ (A) was the only binder phase at 800 °C for the undiluted binder, $Al(PO_3)_3$ (B) was the only binder phase in the presence of AlN or Al_2O_3. No binder phase was observed in the presence of SiC. This may be due to the reaction of the binder with AlN or Al_2O_3 at low temperatures, or with SiC at 510 °C. It is expected that all the binder reacted with AlN, SiC or Al_2O_3 in the case of a binder/carrier ratio of 1/45, even though no reaction product or binder phases were observed by XRD for all preforms prepared with a binder/carrier ratio of 1/45 (Fig. 14). However, the binder-reinforcement reactivity had little effect on the mechanical properties of Al/AlN, Al/SiC or

Al/Al_2O_3 composites due to the small amount of binder used.

The relative reactivity and relative amounts of the binder phases for the phosphate binder and various kinds of reinforcements were obtained and shown in Table XII, based on the methods in [1–4]. The relative reactivity of each reaction product was measured by dividing the sum of the intensities of all XRD peaks from that reaction product by the sum of the intensities of all peaks from the particular reinforcement (i.e. AlN, SiC or Al_2O_3). The relative binder amount was obtained by summing the contributions from all binder phases, such that the relative amount of each phase was measured by dividing the sum of the intensities of all XRD peaks from that phase by the sum of the intensities of all peaks from the particular reinforcement. The total relative reactivity (or total relative binder amount) was obtained by the sum of all relative reactivities (or relative binder amounts) of all reaction products (or all binder phases).

As shown in Table XII, the undiluted binder (containing no reinforcement) was amorphous at room temperature and was crystalline at elevated temperatures ($\geq 200\,^{\circ}C$). The binder phases were aluminium metaphosphates, $Al(PO_3)_3$ (A) and $Al(PO_3)_3$ (B), at both 200 and 510 °C. However the binder phase was $Al(PO_3)_3$ (A) only at 800 °C. At the expense of $Al(PO_3)_3$ (B), the amount of $Al(PO_3)_3$ (A) increased with increasing temperature. Both $Al(PO_3)_3$ (A) and $Al(PO_3)_3$ (B) were present in this work at 200 and 510 °C. In contrast, the undiluted binder in [1–4] exhibited only $Al(PO_3)_3$ (A) at 500 °C and was amorphous even at 200 °C. This small difference in binder phase may be due to the method of drying the binder. In the present work, a small amount of binder was used, so that it could be dried completely, whereas the binder was not totally dried in [1–4]. Moreover, the particulate preform provided more reinforcement surface area than the whisker preform for more efficient binder drying.

The relative reactivity between AlN and the phosphate binder basically increased with increasing heating temperature. At 25°C, AlN reacted with the phosphate to form cristobalite $AlPO_4$, such that it exhibited the highest binder-reinforcement reactivity among the three reinforcements at 25 °C. The relative reactivity of AlN with the phosphate binder remained essentially unchanged from room temperature to 200 °C, but increased from 200 to 510 and to 800 °C. No binder phase was observed at room temperature and 200 °C, while similar amounts of binder phase, $Al(PO_3)_3$ (B), existed at both 510 and 800 °C. Most of

TABLE XII Relative reactivity and relative amount of the binder in various preforms[a]

Reinforcement	25 °C	200 °C	510 °C	800 °C
Undiluted binder, no reinforcement	[M]	(Cr): none (Ber): none (A)/(B) = 0.714/1	(Cr): none (Ber): none (A)/(B) = 0.839/1	(Cr): none (Ber): none (A)/(B) = 1/0
AlN	(Cr): 0.206 (Ber): none S_r: 0.206 (A): none (B): none S_b: 0.0	(Cr): 0.213 (Ber): none S_r: 0.213 (A): none (B): none S_b: 0.0	(Cr): 0.248 (Ber): none S_r: 0.248 (A): none (B): 0.089 S_b: 0.089	(Cr): 0.296 (Ber): none S_r: 0.296 (A): none (B): 0.091 S_b: 0.091
SiC	(Z): none S_r: 0.0 (A): none (B): none S_b: 0.0	(Z): 0.024 S_r: 0.024 (A): none (B): none S_b: 0.0	(Z): 0.205 S_r: 0.205 (A): none (B): 0.051 S_b: 0.051	(Z): 0.217 S_r: 0.217 (A): none (B): 0.061 S_b: 0.061
Al_2O_3	(Cr): none (Ber): none S_r: 0.0 (A): none (B): none S_b: 0.0	(Cr): 0.038 (Ber): 0.285 S_r: 0.323 (A): none (B): none S_b: 0.0	(Cr): 0.216 (Ber): 0.091 S_r: 0.307 (A): none (B): none S_b: 0.0	(Cr): 0.209 (Ber): none S_r: 0.209 (A): none (B): 0.150 S_b: 0.150
SiC_w[b]	[M]	[M]	(Z): 0.141 S_r: 0.141 (A): 0.057 (B): none S_b: 0.057	(Z): 0.189 S_r: 0.189 (A): 0.050 (B): none S_b: 0.050
Undiluted binder[b], no reinforcement	[M]	[M]	(Cr): none (Ber): none (A)/(B) = 1/0	(Cr): none (Ber): none (A)/(B) = 1/0

[a] Reaction products: (Cr), cristobalite $AlPO_4$; (Ber), Berlinite $AlPO_4$; (Z), SiP_2O_7 (15-564 & 15-563); [M], amorphous. Binder phases: (A), $Al(PO_3)_3$ (A); (B), $Al(PO_3)_3$ (B). S_r, total (summation of) relative reactivity; S_b, total relative amount of all binder phases.
[b] From [1–4].

the phosphate binder reacted with AlN to form the reaction product, cristobalite $AlPO_4$, so that relatively little binder phase remained at all temperatures.

Although the relative reactivity between Al_2O_3 and the phosphate was small at room temperature, Al_2O_3 exhibited a higher relative reactivity at 200 °C than AlN. For Al_2O_3, the total relative reactivity decreased with increasing heating temperature from 200 to 510 or to 800 °C. This means that most reaction occurred at 200 °C by the formation of mainly berlinite $AlPO_4$ and a little cristobalite $AlPO_4$. No further reaction of Al_2O_3 with the phosphate binder occurred upon heating from 200 to 510 or to 800 °C. At 510 or 800 °C, the relative reactivity apparently decreased, probably due to a phase transformation from berlinite $AlPO_4$ at 200 °C to cristobalite $AlPO_4$ at 510 or 800 °C.

The relative reactivity between SiC and the phosphate also increased with increasing heating temperature. However, SiC exhibited the least relative reactivity among the three kinds of reinforcements, except at 800 °C. No binder phase was observed at room temperature and 200 °C, while similar amounts of binder phase, $Al(PO_3)_3$ (B), existed at both 510 and 800 °C. Most binder reacted with SiC, so that little binder was left. Compared to the relative relativity of SiC_w in [1–4] (also shown in Table XII), the relative reactivity was higher for particulate SiC (this work) at 510 and 800 °C. This is probably due to the fact that SiC_w has higher crystallinity than SiC_p (SiC particles).

The AlN–binder reactivity at room temperature was probably the largest, followed by Al_2O_3, and then SiC, as only AlN reacted with the phosphate binder during mixing at room temperature. Although Al_2O_3 exhibited the highest total relative reactivity and the highest preform compressive strength (Table V), Al/Al_2O_3 exhibited the lowest composite strength. This may be due to the particle clustering as well as the highest relative reactivity. The use of a binder should be minimized in view of the reactivity.

3.2. Role of preform baking

Preform baking conditions are particularly critical if the reinforcement is moisture sensitive or easy to oxidize. As shown in Tables IX and X, the preform baking condition at 510 °C in vacuum or at 200 °C in air resulted in AlN composites of higher thermal conductivity but of similar tensile properties. This indicates that the preform baking conditions (or Al–AlN interface cleanliness) is more important to the thermal conductivity than to the mechanical properties of AlN composites. For moisture or oxidation-resistant reinforcements, such as SiC, little effect of reinforcement cleanliness on either mechanical or thermal conducting properties was observed.

In view of processing cost and composite thermal conductivity, the preform baking condition of 200 °C in air represents an optimum for fabricating high volume fraction Al/AlN composites. Such a preform baking condition results in Al/AlN composites with similar mechanical properties, but higher thermal conductivities compared to composites with their preforms baked in air at higher temperatures. In contrast, the preform baking condition of 500 °C (not 200 °C) in air represents an optimum for fabricating Al/SiC_w composites of good mechanical properties [1–4]. The difference in the optimum baking condition between AlN particle preforms and SiC whisker preforms is mainly due to the smaller amount of binder used in the former case (i.e. 0.1 wt % phosphate binder in AlN particle preforms against 3–5 wt % phosphate binder in SiC whisker preforms). The small binder amount makes the binder–reinforcement and binder–matrix reactions not important, so that the optimum preform baking temperature is unrelated to the optimum reaction temperature. This means that the preform baking in the case of preforms with a small binder amount is not for the purpose of causing these reactions, but rather is merely for drying the preforms. For Al/SiC_w, the optimum baking temperature of 500 °C corresponded to the development of optimum bonding between the phosphate binder and SiC whiskers [1–4]. On the contrary, for Al/SiC_p and Al/AlN_p, the optimum preform baking temperature of 200 °C corresponded to the attainment of dried preforms. The use of acetone instead of water provided a faster way of preform drying, so acetone is preferred to water, though it is environmentally less desirable. As shown in Fig. 3, the drying of the phosphate binder was achieved at 200 °C. The phosphate binder had similar crystallity at 200 and 500 °C.

3.3. Binder and preform fabrication technique for particulate preforms against whisker preforms

The choice of binder is the first important issue in preform technology. Silica colloid is the most commonly used binder for preform fabrication. In [1–4], the acid phosphate binder was demonstrated to give better mechanical properties for both preforms and the Al/SiC_w composites than the silica binder. The benefit of using the phosphate over the silica colloid was attributed to higher binder–reinforcement reactivity and the nature of the binder phases [1–4]. However, the beneficial attribute offered by the use of the phosphate is less critical in whisker- or short-fibre-reinforced MMCs than particle-reinforced MMCs, as a large amount of binder could be used in the former case without sacrificing the ease of metal infiltration. The benefit of using the phosphate as the binder is more significant for particle reinforcements than whisker or fibre reinforcements, as the phosphate provides a larger binding strength than silica colloid at the same amount.

The binder amount is the second issue in preform technology. The amount of binder used should not block the passage of liquid metal infiltration. This is more important for particulate reinforcements than whisker- or short-fibre reinforcements. The amount of binder used in the whisker or fibre preform was as large as 5 wt % of the preform [1–4], while the optimum amount of binder used in this work was only 0.1 wt %. In general, the optimum amount of binder

decreases with increasing volume fraction of the reinforcement.

The interaction of the carrier with the binder and with the reinforcement is the third important issue in preform technology. The carrier should not cause any flocculation or segregation of the reinforcement in the slurry or the preform, as this would cause incomplete infiltration during MMC fabrication. In this work, the use of silica colloid together with water or acetone as the carrier resulted in incomplete infiltration or non-infiltration in the Al/AlN or Al/SiC composites due to the flocculation problem. In contrast, the use of the phosphate binder and acetone as the carrier led to no flocculation and resulted in good mechanical properties for both AlN and SiC preforms and for the resulting composites.

The preform fabrication technology relies on the combined effect of the binder, reinforcement, carrier and the interactions among these. For moisture- or oxidation-sensitive reinforcements, the preform baking temperature should be minimized in order to avoid oxidation, particularly if the oxide is lower in thermal conductivity than the original reinforcement and a high conductivity is desired.

The discussion in the last section was based on the investigation of the use of the undiluted acid phosphate binder together with each kind of reinforcement. In practice, a very small amount of binder (in this work, 0.1 wt % of the preform) is sufficient to maintain the rigidity of the particulate preform during liquid metal infiltration. This small amount of phosphate binder is expected to lead to negligible binder–reinforcement reaction and negligible binder–matrix reaction. In particular, no binder–matrix reaction (which would produce AlP) was observed in this work, whereas AlP was observed in the case of a large binder amount (namely 3–5 wt % binder in the preform) in the SiC whisker preforms of [1–4]. On the other hand, with the undiluted binder, the binder–SiC reaction (which produced $Si_2P_2O_7$) was observed in both this work and [1–4]. This is because of the large reinforcement volume fraction in this work, so that the binder–reinforcement reaction was observed in spite of the small amount of binder used. The products of the binder–reinforcement and binder–matrix reactions act as *in situ* binders that add to the binding action [1–4], thereby enhancing the high temperature resistance of the composite in the case of [1–4], which used a large binder amount. However, in this work due to the small binder amount, the *in situ* binders were so small in amount that their effects may be neglected.

The thermal conductivity of MMCs may be improved by proper selection of the metal matrix, proper selection of the ceramic reinforcement and by having a clean interface for intimate bonding between the matrix and the reinforcement. In this work, both pure aluminium and AlN were used to satisfy the first two criteria, as both have high thermal conductivity. Although not used in this work, high-grade single crystalline SiC particles, which have similar thermal conductivity as AlN particles, may also be used. In this work, SiC of moderate thermal conductivity ($90\ W\ m^{-1}\ K^{-1}$) was used. In order to obtain a cleaner interface, the contamination of the oxide or oxynitride layer (which is less conducting) in the AlN surface must be controlled to a minimum. Between SiC and AlN, AlN is more prone to oxidation because of its reactivity with moisture ($AlN + H_2O \rightarrow Al_2O_3 + NH_3$). AlN may be contaminated during preform forming and preform baking. In this work, it was observed (Table XIII), that the thermal conductivity of Al/AlN was improved up to 13% by proper preform baking. Al/SiC composites exhibited no improvement by changing the preform baking condition because of the inert nature of SiC. As shown in Table XIII Al/AlN (58 vol % AlN), the preform of which was baked at 200 °C in air, exhibited similar modulus and ductility as the composite with the preform baked at 510 °C in air. The tensile strength of Al/AlN may be slightly improved due to preform baking at 200 instead of 510 °C. For AlN, which is moisture- and oxidation-sensitive, the preform baking conditions (at 200 °C in air or at 510 °C in vacuum) led to cleaner AlN particle surface and Al–AlN interface and resulted in an Al/AlN composite of thermal conductivity up to 87% of the ROM prediction. The AlN preform baked at 510 °C in air resulted in an Al/AlN composite of thermal conductivity equal to 73% of the ROM prediction. No change in the mechanical properties of Al/AlN resulted from the difference in preform baking conditions. For SiC, which is inert, preform baking at 510 °C either in air or in vacuum led to Al/SiC of similar thermal and mechanical properties.

This work provides the first comprehensive study of the fabrication and characterization of high-volume-fraction (up to 75 vol % reinforcement) composites by vacuum infiltration of liquid metal. The factors studied include preform preparation and properties, as well as correlation with the MMC properties.

TABLE XIII Comparison of measured against calculated (ROM) thermal conductivity of Al/AlN and Al/SiC composites[a]

Volume fraction	Measured thermal conductivity ($W\ m^{-1}\ °C$)	Measured value / ROM prediction
0 vol % AlN	211.8 (6.4)[b]	–
60.0 vol % AlN	133.7 (13.5)	0.73
62.7 vol % AlN	129.2 (8.6)	0.71
64.6 vol % AlN	128.7 (3.8)	0.64
100 vol % AlN	163[c]	–
58.0 vol % AlN (in air, 200 °C)	158.0 (6.1)	0.87
59.0 vol % AlN (in vacuum[e], 510 °C)	156.9 (11.2)	0.86
55.0 vol % SiC	125.6 (3.1)	0.87
55.0 vol % SiC (in vacuum[e], 510 °C)	130.2 (7.5)	0.90
100 vol % SiC	90[d]	–

[a] Preforms were baked in air at 510 °C, unless stated otherwise.
[b] Standard deviation shown in parentheses.
[c] Thermal conductivity obtained from Advanced Refractory Technologies, Inc.
[d] Thermal conductivity obtained from Electro Abrasives, Inc.
[e] $\sim 10^{-3}$ torr.

Preforms were studied to understand the effect of the binder composition and reactivity, the effect of the preform heat treatment, and the relationship between the preform processing and the preforms' compressive strength and failure mode. The MMC properties studied included the tensile strength, Young's modulus, ductility and thermal conductivity.

This work has shown that Al/AlN$_p$ (little studied by previous workers) is superior to Al/SiC$_p$ (extensively studied by previous workers) in thermal conductivity and ductility. The superior thermal conductivity of Al/AlN is due to the higher thermal conductivity of AlN itself compared to SiC itself (at least for the conventional grades of AlN and SiC particles used). The superior ductility of Al/AlN is due to the better filler–matrix bonding resulting from the non-reactivity between Al and AlN, in contrast to the reactivity between Al and SiC. Due to the non-reactivity between Al and AlN, Al/AlN is also superior to Al/SiC in the high temperature resistance and shear strength, as shown in a related publication [11].

4. Conclusions

The method of vacuum infiltration of liquid aluminium under an argon gas pressure up to 41 MPa and the use of an improved preform technology were shown to result in metal–matrix composites of high reinforcement volume fractions (from 55 to 75%). At least for Al/AlN, the porosity of the composite decreased with increasing infiltration pressure up to 41 MPa, and increasing the binder/carrier ratio from 1/45 to 1/10 resulted in incomplete or no infiltration of liquid aluminium into the preforms. Among the three reinforcements (AlN, SiC and Al_2O_3) used in this research, Al_2O_3 preforms were the least amenable to being infiltrated due to severe particle clustering and they yielded composites of the poorest tensile properties. The use of the acid phosphate binder, instead of the widely used silica binder, resulted in AlN or SiC particulate preforms with mechanical rigidity and ease of liquid infiltration. The optimum amount of the phosphate binder was limited to 0.1 wt %. A similar amount of silica colloid binder resulted in preforms and metal–matrix composites with inferior mechanical properties due to incomplete infiltration.

The reaction products and reactivity of the acid phosphate binder with three kinds of reinforcements (AlN, SiC and Al_2O_3) were investigated. The acid phosphate binder was in the form of type A and B aluminium metaphosphate ($Al(PO_3)_3$) at 200 or 510 °C and in the form of type A aluminium metaphosphate ($Al(PO_3)_3$) at 800 °C. Type A aluminium metaphosphate ($Al(PO_3)_3$) is more stable at high temperatures than type B. AlN particles reacted with the undiluted phosphate binder to form cristobalite $AlPO_4$ upon mixing at room temperature and during subsequent heating at 200, 510 or 800 °C. At room temperature, AlN particles had the highest total relative reactivity with the undiluted acid phosphate binder. Al_2O_3 had the highest total relative reactivity with the acid phosphate at 200 °C, forming predominantly berlinite $AlPO_4$ and cristobalite $AlPO_4$. The cristobalite $AlPO_4$ increased at the expense of berlinite $AlPO_4$. At 800 °C, only cristobalite $AlPO_4$ was present. The Al_2O_3 preforms hence exhibited the highest compressive strength.

The preform baking environment and temperature were particularly critical to the thermal conductivity of Al/AlN composites, as AlN was moisture- and oxidation-sensitive. An optimum baking condition (at 200 °C in air or 510 °C in vacuum), which resulted in AlN particle surface cleanliness and hence Al–AlN interface cleanliness, was obtained. The preform baking condition was less critical to the mechanical properties. For Al/SiC, the baking condition did not affect the mechanical properties or the thermal conductivity, as SiC was relatively inert. Under proper preform baking conditions, the thermal conductivity of Al/AlN and Al/SiC reached 87 and 90%, respectively, of the theoretical values based on Rule of Mixture (ROM).

Acknowledgements

This work was supported by the Advanced Research Projects Agency of the US Department of Defense and by the Center for Electronic and Electro-Optic Materials of the State University of New York at Buffalo.

Appendix 1

Fig. 28a shows the weight change against time, and temperature against time curves of AlN and SiC powders heated from 100 to 1000 °C. The weight changes of AlN and SiC were monitored using a Perkin Elmer TGA7 thermogravimetric analyser, which was sensitive to $\pm$ 0.001 mg. The AlN or SiC powder was placed in the platinum sample boat and the furnace was purged with a constant flow of compressed air at 20 $cm^3 min^{-1}$. The furnace temperature was maintained at 100 °C for 30 min, raised up to either 500 or 1000 °C at a heating rate of 20 °C min^{-1}, and then maintained isothermally at either 500 or 1000 °C for 5–10 h. Both AlN and SiC powders decreased in weight during the initial heating at 100 °C because of the loss of moisture. During heating from 100 to 1000 °C (Fig. 28b), AlN powder started oxidation at about 600 °C with an onset of 884 °C. On the other hand, SiC powder lost weight with an onset of 691 °C due to the oxidation of residue carbon inside the SiC powder, and then started to gain weight at about 878 °C due to the oxidation of SiC.

When maintained isothermally at 500 °C in air, as shown in Fig. 28c, the AlN also exhibited a weight increase, indicating oxidation of the AlN powder at 500 °C. The initial oxidation rate (the slope of the curve of weight change against time) was $10^{-4} h^{-1}$. This is in contrast to the observation [10] that AlN is inert to atmospheric air at temperatures below 700 °C for 60 h. Thus the AlN in the preform oxidized during preform baking at 500 °C, resulting in more aluminium oxide in the surface of the AlN powder. The weight gain of AlN was 0.1 wt % after heating at 500 °C for 4 h. (As shown in Fig. 14, no oxidation of AlN was detected with XRD after heating the AlN

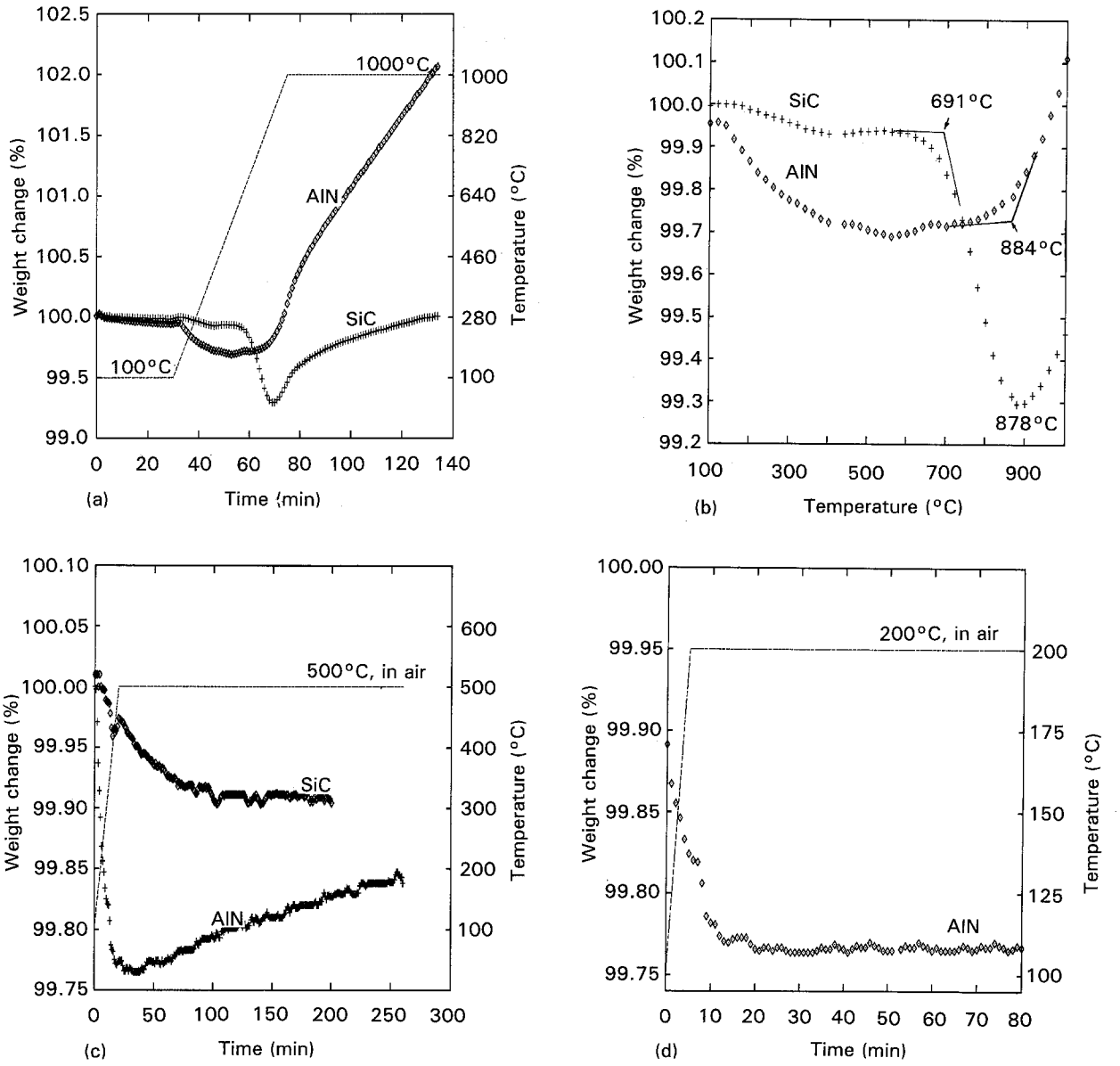

Figure 28 Thermogravimetric analysis curves obtained for AlN and SiC powders at various isothermal temperatures. (a) Samples were maintained at 100 °C for 30 min, heated to 1000 °C at a heating rate of 20 °C min^{-1}, and then maintained at 1000 °C for 1 h. (b) Weight change against temperature curve of (a) during heating from 100 to 1000 °C. (c) Samples maintained at 500 °C for 3–4 h. (d) Samples maintained at 200 °C for 1 h.

preform at 660 °C for 43 h. This may be due to the fact that the thin oxide or oxynitride layer on the AlN particle surface was too thin to be detected by XRD). As shown in Fig. 28d, the AlN exhibited no weight change due to heating in air at 200 °C, indicating no oxidation of AlN at 200 °C. The baking temperature and environment are important to reinforcements which are moisture- or oxidation-sensitive. On the other hand, the SiC exhibited a weight loss due to the oxidation of residual carbon at 500 °C. No oxidation of SiC itself was observed.

References

1. JENG-MAW CHIOU, Ph.D. thesis, State University of New York at Buffalo, 1991.
2. J. M. CHIOU and D. D. L. CHUNG, *J. Mater. Sci.* **28** (1993) 1435.
3. *Idem, ibid.* **28** (1993) 1447.
4. *Idem, ibid.* **28** (1993) 1471.
5. R. C. PROGELHOF, J. L. THRONE and R. R. RUETSCH, *Polym. Engng Sci.* **16** (1976) 615.
6. M. K. AGHAJANIAN, J. T. BURKE, D. R. WHITE and A. S. NAGELBERG, *SAMPE Q.* **20** (1989) 43.
7. S.-Y. OH, J. A. CORNIE and K. C. RUSSELL, *Met. Trans. A* **20A** (1989) 527.
8. J. C. VIALA, P. FORTIER and J. BOUIX, *J. Mater. Sci.* **25** (1990) 25.
9. Z. HASHIN and S. SHTRIKMAN, *J. Mech. Phys. Solids* **11** (1963) 127.
10. A. D. KATNANI and K. I. PAPATHOMAS, *J. Vac. Sci. Tech.* **5** (1987) 1335.
11. SHY-WEN LAI and D. D. L. CHUNG, *J. Mater. Sci.*, in press.

Received 16 September
and accepted 30 November 1993